

23 November 1979 • Vol. 206 • No. 4421

SCIENCE

AMERICAN ASSOCIATION FOR THE ADVANCEMENT OF SCIENCE



Reports

Voyager 2 Encounter with the Jovian System

Abstract. An overview of the Voyager 2 encounter with Jupiter is presented, including a brief discussion of the trajectory, the major sequence modifications performed because of the Jupiter measurements obtained with Voyager 1, and highlights of the results that are described in the subsequent reports.

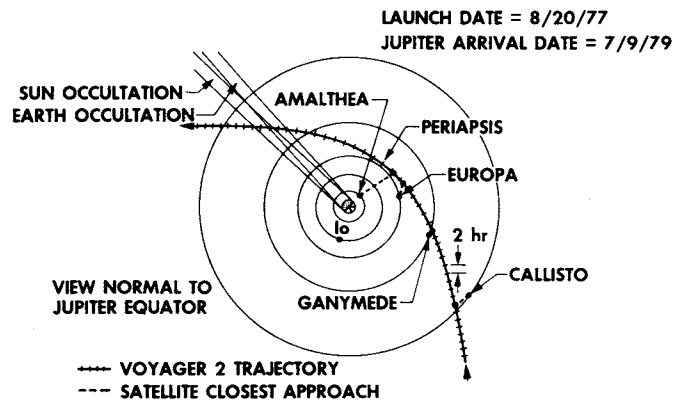
The Voyager 2 encounter with Jupiter was the second step in the NASA Voyager Program of exploration of the outer planets. Launched on 20 August 1977, Voyager 2 arrived at Jupiter just 18 weeks after the successful Voyager 1 flyby (1). Voyager 2 began extensive Jovian measurements on 25 April 1979, encountered Jupiter at the closest approach distance of 721,670 kilometers at 22:29.0 UTC (Universal Time, coordinated) 9 July 1979, and completed its principal measurements of Jupiter's environment on 5 August 1979. Throughout this 103-day period, nearly continuous measurements were obtained from the Jovian system and the nearby interplanetary medium, enabling a number of discoveries to be made and providing additional information on the Voyager 1 studies.

The Voyager 2 scientific investigations and instruments are listed in Table 1. The location of the instruments and the essential characteristics of the spacecraft

were given in the Voyager 1 Jupiter report (1).

The timing of the Jupiter encounter was chosen so that the Voyager 2 encounter with Saturn would occur during a period when the planetary positions would permit the spacecraft to swing by Saturn and continue toward a Uranus en-

Fig. 1. Voyager 2 Jupiter encounter geometry. This view from the planet north pole shows the trajectory closest approach geometry to the planet and selected satellites, 2-hour time interval tick marks along the trajectory path, and Earth and sun occultation zones through which the spacecraft flies. The actual closest approach distances are listed in Table 2.



counter in 1986. This arrival date also resulted in a larger flyby distance at Jupiter with a correspondingly lower radiation dose than Voyager 1 received from the intense radiation nearer the planet.

The specific Voyager 2 encounter trajectory was chosen to complement that of Voyager 1. A view of the Voyager 2 trajectory through the Galilean satellite system is shown in Fig. 1, which covers ± 44 hours around closest approach to Jupiter. Special characteristics of the Voyager 2 trajectory are: (i) a close approach to Europa, which was observed only at a great distance from Voyager 1; (ii) close approaches to Ganymede and Callisto prior to Jupiter closest approach, thus providing a high resolution view of the opposite faces from those observed by Voyager 1; (iii) an outbound direction that allowed the deepest penetration to date of the Jovian magnetotail (see Fig. 2); (iv) Earth and sun occultations which probe the south polar Jovian atmosphere for comparison with the equatorial occultations by Voyager 1; and (v) a higher approach latitude to provide a different view of the latitude-de-

Table 1. Scientific investigations for the Voyager mission.

Investigation*	Abbreviation	Typical Jovian encounter objectives
Imaging science (B. A. Smith)	ISS	High-resolution reconnaissance over large phase angles; atmospheric dynamics; geologic structure of satellites
Infrared radiation (R. A. Hanel)	IRIS	Atmospheric composition, thermal structure, and dynamics; satellite surface composition and thermal properties
Photopolarimetry (C. W. Hord)	PPS	Atmospheric aerosols; satellite surface texture and sodium cloud
Radio science (V. R. Eshleman)	RSS	Atmospheric and ionospheric structure, constituents, and dynamics
Ultraviolet spectroscopy (A. L. Broadfoot)	UVS	Upper atmospheric composition and structure; auroral processes; distribution of ions and neutral atoms in the Jovian system
Magnetic fields (N. F. Ness)	MAG	Planetary magnetic field; magnetospheric structure; Io flux tube currents
Plasma particles (H. S. Bridge)	PLS	Magnetospheric ion and electron distribution; solar wind interaction with Jupiter; ions from satellites
Plasma waves (F. L. Scarf)	PWS	Plasma electron densities; wave-particle interactions; low-frequency wave emissions
Planetary radio astronomy (J. W. Warwick)	PRA	Polarization and spectra of radio frequency emissions; Io radio modulation process; plasma densities
Low-energy charged particles (S. M. Krimigis)	LECP	Distribution, composition, and flow of energetic ions and electrons; satellite-energetic particle interactions
Cosmic-ray particles (R. E. Vogt)	CRS	Distribution, composition, and flow of high-energy trapped nuclei, energetic electron spectra

*The principal investigator or team leader is indicated in parentheses.

Table 2. Selected Jovian and Voyager encounter parameters. Except as noted, the satellite physical data are from (4). Distances are to the center of mass, not to the body surface.

Body	Mean distance from Jupiter (10^3 km, R_J)*		Mean orbital period (days)	Mass (moon = 1)†	Closest approach distance (km) from	
					Voyager 1	Voyager 2
Jupiter				318.1‡§ (Earth = 1)	348,890	721,670
Amalthea (J5)	181.3, 2.54	0.489			420,200	558,370
Io (J1)	421.6, 5.90	1.769	1.21		20,570	1,129,900
Europa (J2)	670.9, 9.40	3.551	0.66		733,760	205,720
Ganymede (J3)	1070.0, 14.99	7.155	2.03		114,710	62,130
Callisto (J4)	1880.0, 26.33	16.689	1.45		126,400	214,930

* $R_J = 71,398$ km = Jupiter equatorial radius (5). †Mass of moon = 7.350×10^{22} kg (6). ‡Mass of Earth = 5.976×10^{24} kg (6). §Mass of Jupiter = 1.901×10^{27} kg (5).

pendent radio emissions observed by Voyager 1. Important characteristics of the two Voyager trajectories are summarized in Table 2, which also contains some relevant parameters of the Jovian system (2). Together Voyager 1 and 2 establish a 7-month time base for the study of atmospheric dynamics and an even longer time base for Io plasma torus studies.

In order to derive additional information on some of the Voyager 1 discoveries, a number of changes were made to the preplanned Voyager 2 sequences (3). For example, a number of image sequences of the Jovian ring system were inserted into the timeline to determine the radial extent of the ring, and a 10-hour period of repetitive imaging of Io was added in order to search for any short-term variations in the volcanic plumes. In addition, ultraviolet scans of the Jovian auroral regions were modified so that the region of maximum activity could be accurately determined, infrared observations of the polar regions were modified to optimize the study of global distribution of ethane and acetylene, and more high-rate plasma wave and radio measurements were scheduled for lightning and other studies. Other modifications included several additional rolls of the spacecraft for plasma studies, a redesign of the ultraviolet observations of the Io torus in order to record any temporal variations, and the addition of a stellar occultation of Jupiter for study of the upper atmosphere.

Both the originally planned sequences and the subsequent modifications had to take into account the presence of a backup mission load in one-half of one of the two sequencing memories. This minisequence for spacecraft and science data acquisition at Saturn was designed to automatically take control should the failure of the single remaining command receiver prevent the spacecraft from receiving further sequencing instructions

from Earth (the other command receiver failed during the preencounter cruise period). The design and duration of the originally planned sequences and their uplinking to the spacecraft also had to take into account the fact that the failure of a component had increased the sensitivity of the remaining command receiver to thermal changes and radiation dose. The impact of these constraints on the scientific return from Voyager 2 was minimized by careful design and implementation of the sequences and by the development and execution of appropriate operational procedures.

Like Voyager 1, Voyager 2 returned data on a broad range of scientific studies as discussed in the following reports. The Voyager 2 encounter has not only

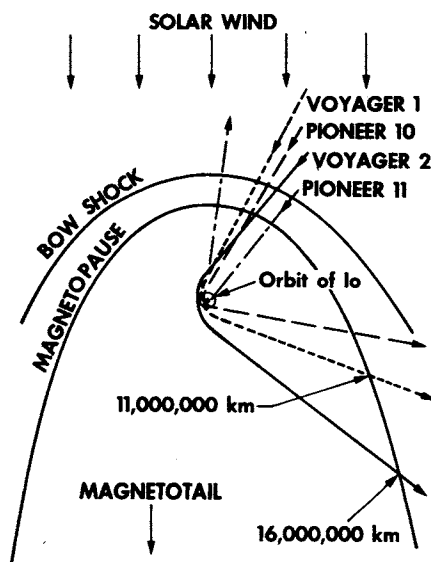


Fig. 2. North polar view of the Jovian magnetosphere region. The trajectories of the four Pioneer and Voyager spacecraft that have examined Jupiter are shown for a fixed bow shock and magnetosphere configuration. All four spacecraft have sampled the sunward bow shock and magnetosphere region at various latitudes, but only limited magnetotail probing has occurred, with Voyager 2 remaining in the tail for the greatest distance from Jupiter.

provided additional details about a number of the Voyager 1 discoveries but has also enabled additional discoveries to be made. Some highlights from the subsequent reports are as follows.

Atmosphere

The main atmospheric jet streams were present during both Voyager encounters, with some change in velocity.

The Great Red Spot, the white ovals, and the smaller white spots at 41°S appear to be meteorologically similar.

The formation of a structure east of the Great Red Spot formed a barrier to the flow of small cloud vortices which earlier were circulating about the Great Red Spot.

The ethane (C_2H_6) to acetylene (C_2H_2) abundance ratio appears to be larger in the polar regions than at lower latitudes and appears to be 1.7 times higher on Voyager 2 than on Voyager 1.

Thermal maps at ~ 150 and ~ 800 millibars of atmospheric depth exhibit both local and large-scale structure and suggest the importance of dynamical heating and cooling processes.

A map of Jupiter at 2400 \AA shows the distribution of ultraviolet absorbing haze. The polar regions are surprisingly dark, suggesting absorbing material must be above the 40-millibar level.

Equatorial ultraviolet emissions indicate planet-wide charged particle precipitation.

The high-latitude ultraviolet auroral activity occurs on the magnetic field lines which thread the plasma torus.

Ionospheric temperatures in the south polar region were 1200 K and 1600 K, the latter being the highest topside plasma temperature observed at Jupiter.

Satellites and Ring System

The ring consists of a bright, narrow segment surrounded by a broader, dimmer segment ~ 5800 km wide.

Upper limits on the optical depth of the ring material range from 3×10^{-4} to 3×10^{-3} in the infrared.

The interior of the ring is filled with much fainter material that may extend down to the top of the atmosphere.

Images of Amalthea in silhouette against Jupiter indicate that the satellite may be faceted or diamond shape.

Volcanic activity on Io had changed somewhat, with six of the plumes observed by Voyager 1 still erupting.

The largest Voyager 1 plume had ceased, while the dimensions of another plume had increased by 50 percent.

Several large-scale changes in Io's appearance had occurred, consistent with

surface deposition rates of 10^{-2} centimeters per year deduced for plume areas.

The surface of Europa is remarkably smooth with few craters and is probably 10^8 years or older.

The surface of Europa consists of slightly mottled terrain and uniformly bright terrain crossed by linear markings and ridges.

There are four basic terrain types on Ganymede, including younger, smooth terrain and a rugged impact basin that was observed by Voyager 2.

Callisto's entire surface, which is even more densely cratered in the hemisphere viewed by Voyager 2, must be some 4×10^9 years old.

Low latitude surface temperatures on the Galilean satellites range from 80 K (night) to 155 K (the subsolar point on Callisto).

Underneath a thin surface layer, the thermal inertia of Callisto is about twice that of the moon.

Magnetosphere

The outer region of the magnetosphere contains a hot plasma consisting primarily of hydrogen, oxygen, and sulfur ions.

The hot plasma generally flows in the corotation direction out to the boundary of the magnetosphere.

The plasma sheet, which inside of ~ 50 Jupiter radii (R_J) lies in the magnetic equatorial plane, is approximately parallel to the Jovian or the solar magnetosphere equatorial plane at greater tailward distances.

Between 18 and 25 R_J , the bulk velocity of the low energy plasma is lower than the corotation value.

Electron densities as low as $\sim 10^{-5}$ per cubic centimeter occur on the predawn taillike region of the magnetosphere.

Beyond $\sim 160 R_J$, the hot plasma streams nearly antisunward.

Outbound the spacecraft experienced multiple magnetopause crossings between 169 and 279 R_J .

The abundance of oxygen and sulfur relative to helium at ~ 1 MeV per nucleon increases with decreasing distance from Jupiter.

The phase space density gradient of higher energy oxygen (~ 6 MeV per nucleon) suggests that these nuclei are diffusing inward toward Jupiter.

At 10 R_J , the Jovian magnetic field intensity was significantly depressed (20 percent low) because of the immersion of Voyager 2 in the current sheet.

The ultraviolet emission from the Io plasma torus was twice as bright as 4 months earlier, and the temperature had decreased by 30 percent to 60,000 K.

The low frequency (kilometric) radio emissions (< 1 MHz) from Jupiter have a strong latitude dependence with a narrow shadow zone near the magnetic equator.

The kilometric radiation often contains narrowband emissions that drift to lower or higher frequencies with time.

Intense narrowband emissions were observed that may be the source of continuum radiation trapped inside the magnetosphere.

A complex magnetosphere interaction with Ganymede was observed in the magnetic field, plasma, and energetic particles up to $\sim 200,000$ km from the satellite.

E. C. STONE

California Institute of Technology,
Pasadena 91125

A. L. LANE

Jet Propulsion Laboratory,
California Institute of Technology

References and Notes

1. A brief overview describing the Voyager spacecraft, its instrument complement, and the Voyager 1 trajectory at Jupiter can be found in *Science* **204**, 945 (1979); other Voyager 1 reports appeared in the same issue.
2. The new values of the satellite radii, as determined by Voyager 1 and 2, are given by B. A. Smith *et al.*, *Science* **204**, 951 (1979), and B. A. Smith *et al.*, *ibid.* **206**, 927 (1979).
3. The sequencing aspect of the spacecraft operation is briefly described in (1).
4. D. Morrison *et al.*, *Introducing the Satellites, Planetary Satellites*, J. A. Burns, Ed. (Univ. of Arizona Press, Tucson, 1977), p. 6.
5. R. Smoluchowski, in *Jupiter*, T. Gehrels, Ed. (Univ. of Arizona Press, Tucson, 1976).
6. C. W. Allen, *Astrophysical Quantities* (Athlone, London, 1973).
7. The extraordinary scientific findings discussed in this issue of *Science* represent the culmination of many years of dedicated, tireless effort by a large number of people at all levels in numerous organizations. The scientists associated with the Voyager Project gratefully acknowledge the superb accomplishments of all these individuals. The Voyager Program is one of the programs of the Planetary Division of NASA's Office of Space Science. The Voyager Project is managed by the Jet Propulsion Laboratory of the California Institute of Technology under NASA contract NAS 7-100.

5 October 1979

The Galilean Satellites and Jupiter: Voyager 2 Imaging Science Results

Abstract. *Voyager 2, during its encounter with the Jupiter system, provided images that both complement and supplement in important ways the Voyager 1 images. While many changes have been observed in Jupiter's visual appearance, few, yet significant, changes have been detected in the principal atmospheric currents. Jupiter's ring system is strongly forward scattering at visual wavelengths and consists of a narrow annulus of highest particle density, within which is a broader region in which the density is lower. On Io, changes are observed in eruptive activity, plume structure, and surface albedo patterns. Europa's surface retains little or no record of intense meteorite bombardment, but does reveal a complex and, as yet, little-understood system of overlapping bright and dark linear features. Ganymede is found to have at least one unit of heavily cratered terrain on a surface that otherwise suggests widespread tectonism. Except for two large ringed basins, Callisto's entire surface is heavily cratered.*

Atmosphere of Jupiter: Introduction. Voyager 2's observations of Jupiter were carried out on a schedule similar to that successfully executed during the Voyager 1 encounter with Jupiter (1). Continuous global observations of the planet were made for a period of 63 days. The sequence began with a multicolored series of narrow-angle frames every 72° of longitude (observatory phase), then changed to one of periodic mosaics when the planet's image became too large to fit within the field of view of the narrow-angle camera. During the final 12 days of approach, selected areas of the planet were targeted for observations that could be used for studies of cloud morphologies and atmospheric motions. The combined Voyager 1 and 2 observations of Jupiter provide an almost continuous record, over a 6-month period, of the behavior of the Jovian atmosphere at a res-

olution far better than can be obtained from Earth-based studies. In this report we briefly describe the changes in the cloud morphologies and local atmospheric motions that have occurred in the Jovian atmosphere between the Voyager 1 (5 March) and Voyager 2 (9 July) encounters.

General appearance and average zonal velocities of the Jovian atmosphere. The Voyager observations show some significant changes in the cloud patterns within a period of only a few months. These changes are in marked contrast with the observations of the two Pioneer spacecraft (2) which, although separated by a period of 12 months, showed little change in the cloud structure. Earth-based studies, however, have shown that cloud structures vary significantly with periods of about 4 to 5 years and occasionally 1 year or less (3).

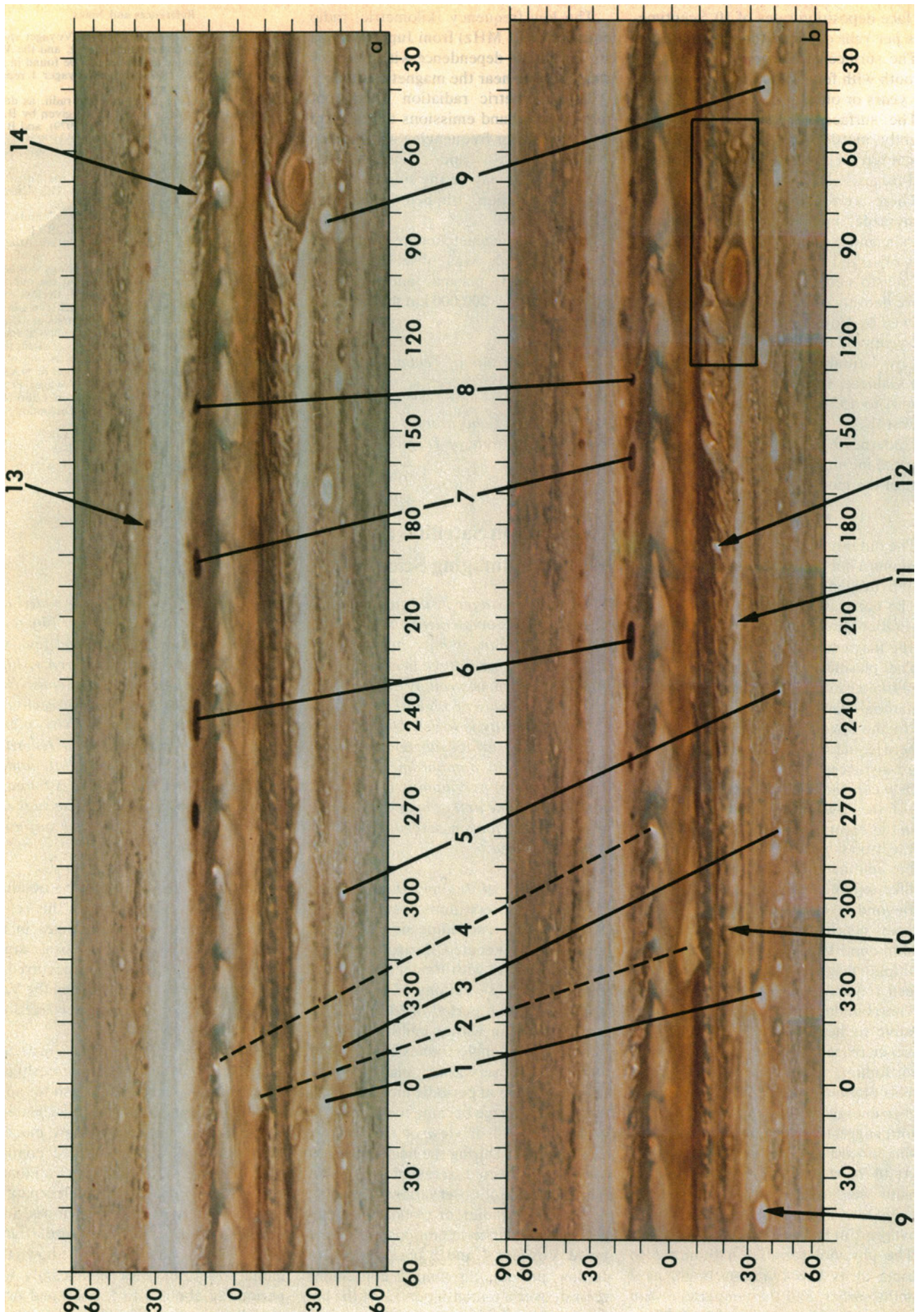


Fig. 1. Cylindrical map projections from Voyager 1 and 2. (a) Voyager 1 data obtained on rotation 65 (1 February) and (b) Voyager 2 data obtained on rotation 349 (23 May). (Rotations are numbered from the first Voyager 1 images on 6 January 1979.) Specific features discussed in the text are labeled 1 to 14 to facilitate recognition. Features 2 and 4 are connected by dashed lines to stress that they reside in the high-speed equatorial jet. The boxed area contains the "recirculating current," which developed during the interval between the Voyager encounters. The longitude scale is in system III and latitudes are planetographic. These mosaics were prepared by J. A. Mosher and E. P. Korsmo at the Jet Propulsion Laboratory (JPL) Image Processing Laboratory.

A comparison of the cylindrical projections for Voyager 1 (1 February 1979) and Voyager 2 (23 May 1979) reveals some of these changes and emphasizes the apparent differences due to differential zonal motion between features (Fig. 1). Features aligned with the Great Red Spot (GRS) at the time of the Voyager 1 encounter have moved to different longitudes 4 months later. The cloud structure around the GRS appears quite different in the two maps. This difference is due, in part, to the chance alignment of the two white ovals (features 1 and 9, Fig. 1) and the intervening high-albedo cyclonic region that was located below the GRS in February. This cloud system has shifted eastward along with the pattern of small anticyclonic ovals at 41°S latitude (features 3 and 5), resulting in a considerable change in the appearance of the GRS. Its size, however, has remained constant between the encounters, measuring 22,000 by 11,000 km.

The South Tropical Zone (STrZ) (feature 11, Fig. 1) (4) has decreased in width, while the zonal extent of the cyclonic region to the west of the GRS has increased between the encounters. During late February, intensely bright clouds emerged in the South Equatorial Belt (SEB) (feature 12), expanded, and drifted toward the GRS. This particular flow has continued to add material to the disturbed region that lies west of the GRS.

Ingersoll *et al.* (5) presented the results of measurements of zonal velocities of cloud features in the Jovian atmosphere computed from displacements of features typically 100 to 200 km in size over time intervals of 10 to 30 hours (one to three Jovian rotations). These results indicate zonal jet structure and, by comparison with Earth-based observations, suggest that the jets are stable over intervals of several years. In order to compare zonal velocity variations with changes in the appearance of the visible

cloud deck, the region of the planet centered on the GRS was chosen for derivation of the comparative velocity profiles presented in Fig. 2. For Voyager 1, this region corresponds to longitudes 330° to 120°W. For Voyager 2, the region is 0° to 150°W. All longitudes are given in system III (1). The measurement technique employed to derive these velocities is identical to that used by Ingersoll *et al.* (5). No attempt has been made to differentiate between motions of clouds at different altitudes; thus, these velocity profiles represent the measured displacement of identifiable cloud features at whatever level they may appear in the visible cloud deck.

Comparison of the velocity profiles in Fig. 2 shows that the main jets are present in the data from both encounters with few significant changes. At the time of

the Voyager 1 encounter, the velocity of the southern edge of the Equatorial Zone (EZ, 7°S) was ~ 150 m/sec, compared with 95 m/sec 4 months later. In February (Voyager 1) the measurements referred to the chevron-shaped features that propagate along this boundary. At the time of the Voyager 2 encounter, a large white cloud (feature 2, Fig. 1) greatly modified the local flows. This is the feature that, during the Voyager 1 encounter, appeared to interact with the cyclonic region west of the GRS, generating a trail of clouds in the SEB. Feature 2 has circled the planet more than twice during the interval between the observations shown in Fig. 1; however, it has moved eastward at a slower rate than the smaller chevron features observed at the same latitude.

The northern edge of the equatorial re-

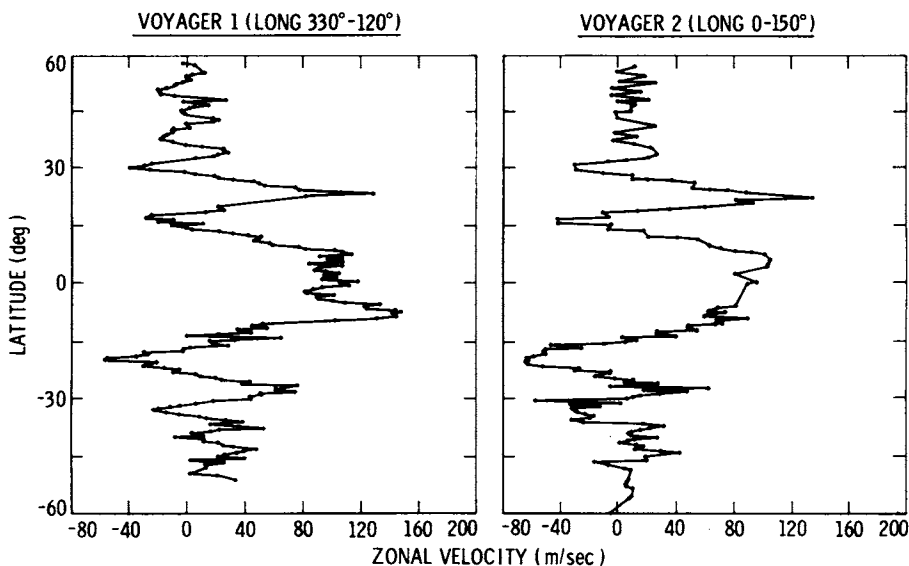


Fig. 2. Velocity profiles from the north polar to the south polar region of Jupiter at a portion of the planet covering 150° of longitude centered on the GRS. Velocity measurements were compiled by tracking cloud features as small as 130 km at 10- to 30-hour intervals (one to three Jovian rotations). Several thousand measurements were used to generate these zonal velocity profiles.

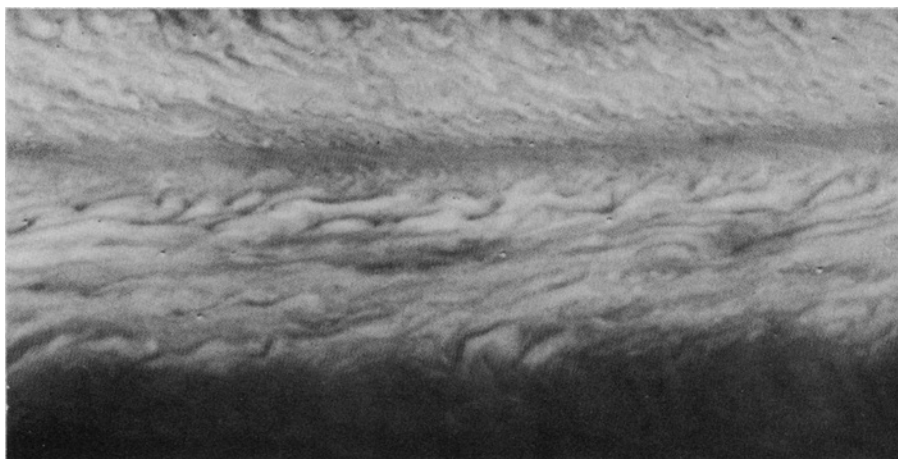


Fig. 3. Train of waves seen along the interface between the NEB and the NTrZ. The wavelength of the disturbance is 700 to 1000 km. This image was taken through a violet filter on rotation 433 (3 July 1979). Distance on Jupiter from top to bottom of the image is approximately 14,000 km.



Fig. 4. Portions of the NTeB, NTrZ, and NEB with the largest of the dark brown clouds that reside in this region. A white cloud is seen moving across the dark brown area, causing the clouds to appear to be at different altitudes. The start of the white cloud formation was evident in the Voyager 1 picture displayed as figure 5a in Smith *et al.* (1). This image was taken on rotation 440 (6 July 1979) and covers a distance (top to bottom) of about 12,000 km.

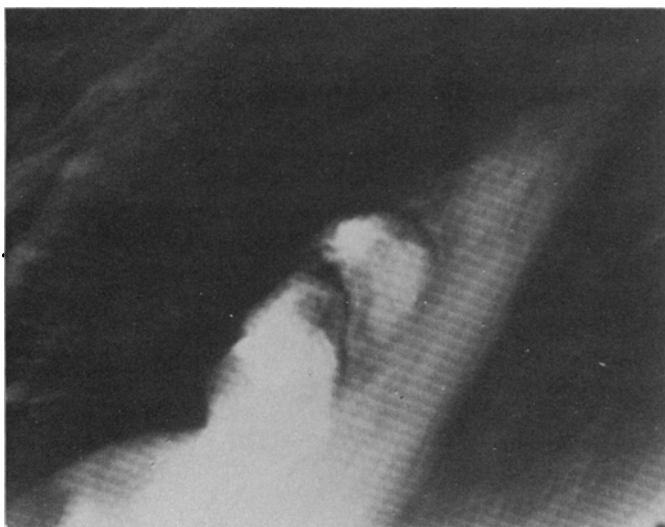


Fig. 5. High-resolution image of a plume nucleus, showing that there are two active areas of convection. The image was taken through a violet filter on rotation 442 (7 July 1979) and includes an area about 10,000 km on a side.

gion also changed between encounters: Voyager 2 showed that the highest-velocity region of the jet (~ 100 m/sec) was situated 2° nearer to the equator at $\sim 7^\circ\text{N}$. At the time of the Voyager 1 encounter, the system of diagonally aligned clouds in the North Equatorial Belt (NEB) (feature 14) was located at the longitude of the GRS, interacting strongly with the flow of the equatorial plumes. This was no longer the case in the Voyager 2 profile, and it may account for the change in the velocity profile for the region 10° to 15°N as well as for the equatorward shift.

The broadening of the retrograde jet between 15° and 22°S is associated with the change in latitudinal extent of the STrZ as well as the pattern of circulation east of the GRS and will be discussed later in this report.

Differences south of 30°S should not necessarily be attributed to real changes in zonal velocities; far fewer measurements have been completed for Voyager 2 than for Voyager 1. Therefore, the average velocities for Voyager 1 data are currently more reliable than those computed from the Voyager 2 data.

The overall picture displayed in Fig. 2 indicates that few velocity changes have

occurred in a longitudinal region centered on the GRS within the time interval between Voyager encounters.

Regional cloud structures. We follow here the procedure of Mitchell *et al.* (6) for Voyager 1 in comparing cloud structures on a region-by-region basis, beginning in the north and progressing southward. In contrast to long-lived large features in the southern hemisphere such as the GRS and white ovals (features 1 and 9, Fig. 1), individual features in the northern hemisphere at 35°N (for example, see feature 13, Fig. 1) have undergone noticeable changes between encounters. The spacing between the features has altered as a result of their variable drift rates so that no major interactions between the features were observed during the Voyager 2 sequences. The disturbed region of the atmosphere to the west of feature 13 has subsided, and the long diagonal structures previously seen in the zone to the south of these clouds have become less pronounced.

The high-speed north temperate jet, seen in the upper half of Fig. 3 at 23°N , has maintained the same visual appearance between the encounters, and the zonal velocities of this region are similar

to those found during the first Voyager encounter (~ 150 m/sec).

The dark brown clouds in the NEB (features 6, 7, and 8, Fig. 1), which move in an eastward direction, have undergone noticeable changes. The dark brown cloud originally west of feature 6 has virtually disappeared in the time between the two encounters. A more noticeable change in feature 6 is apparent in the Voyager 2 high-resolution image, Fig. 4. A white cloud is seen intruding over a portion of this feature; early formation of this feature appears in the Voyager 1 images (7). Overlying the dark cloud itself, wispy cirrus veils of cloud are evident. This observation is particularly important, as it provides direct evidence of the differences in cloud altitudes. The colors of clouds, however, continue to be a major problem of Jovian atmospheric physics and chemistry.

The equatorial region remains characterized by the train of plumes moving in the strong westerly jet along the northern edge. Morphologically, however, there are some important changes in the structure of these features. At the time of Voyager 2 encounter only 11 plumes were seen, compared with the 13 visible during Voyager 1 encounter. Furthermore, Fig. 1 shows that only one of the features had an active bright nucleus (feature 4), which we have interpreted as representative of mesoscale convection (5). A high-resolution image of a plume head observed by Voyager 2 reveals a complicated structure (Fig. 5). The nucleus has two active convective centers that are each suggestive of upward propagation of energy and the divergence of material at the cloud-top level. Voyager 2 data show an absence of the wave patterns observed in the plume tails during Voyager 1 encounter. However, many other examples of small-scale waves have been observed during the second encounter. Within 2° of the equator, trains of waves similar to those in the Voyager 1 data (8) have been observed. Wave patterns were present in the clouds to the northeast of the GRS and may be generated by small-scale convection in this region. At the interfaces of the SEB and EZ and the NEB and NTrZ (North Tropical Zone), trains of waves were frequently observed (for example, see the lower half of Fig. 3). These disturbances, which have a wavelength of ~ 700 to 1000 km and a longitudinal extent of several thousands of kilometers, are common in these regions.

The high-resolution pictures of the GRS, the white ovals (Fig. 6), and the smaller spots at 41°S indicate that they

have similar morphologies, anticyclonic rotations, and disturbed regions to the west of the individual features. In (1) we estimated that the GRS had a vorticity of $2.5 \times 10^{-5} \text{ sec}^{-1}$ and a Rossby number of about 0.2. Using an average tangential velocity and assuming a circular feature with a radius equal to the average value of the major and minor axes of the selected feature, we estimate that for the white ovals these parameters are typically $\sim 3 \times 10^{-5} \text{ sec}^{-1}$ and ~ 0.16 , and for the small ovals at 41°S the values are $2 \times 10^{-5} \text{ sec}^{-1}$ and 0.09. These preliminary results suggest meteorological similarities in these clouds. The major difference between the GRS and these features is simply color. Ingersoll *et al.* (5) suggested that the currents, as opposed to colors, are long-lived features of the Jovian atmosphere; thus these spots may be maintained by deep-seated motions (hundreds of kilometers deep).

The region east of the GRS changed dramatically between the two encounters. At the time of Voyager 1, small cloud vortices moved toward the GRS at a speed of 55 m/sec and made several rotations of the feature. In the time between the encounters, a cloud structure developed east of the GRS and formed a barrier to the flow. The region outlined by a box in Fig. 1 is expanded in Fig. 7 to show a time sequence of images. Cloud vortices, such as feature 10 (Fig. 1), still approached the GRS at about 55 m/sec. However, the presence of the barrier now forced them to recirculate in the direction from which they came. Considerable shear was set up in this region, causing the cloud vortices to become distorted. At times, as many as four cloud vortices could be observed in this recirculating current. Throughout this encounter the rotation of the GRS continued in a manner similar to that observed during the previous encounter.

Those Voyager observations may be significant in providing an understanding of the large-scale changes in the visible cloud structure. It is possible that they show the beginning of a transition to the appearance of the planet as observed by the Pioneer spacecraft 5 years ago, when the GRS resided in apparently featureless surroundings.

Near 40°S the Voyager 1 images revealed a general pattern of anticyclonic ovals alternating longitudinally with cyclones of folded filamentary morphology (6). One exception to this pattern is the spot at 38°S , 85°W in Fig. 1a; it appears as a compact oval while exhibiting the cyclonic vorticity typical of other features at the same latitude that are mostly

filamentary in nature. On 4 May 1979, a small bright core appeared in the oval's center. The bright core expanded longitudinally and was drawn into a bright S-shaped pattern. Within five rotations (Fig. 8) the oval, which had previously remained unchanged for at least 287 rotations, was transformed into a region of folded filaments consistent with the prevailing pattern.

High-altitude hazes. Observations of the limb at large phase angles (for example, 140°) as the spacecraft moved away from Jupiter have revealed evidence of haze layers extending to high levels in the atmosphere. The initial anal-

ysis of Voyager 1 data by Cook *et al.* (9) suggests that the hazes extend to pressures of ~ 3.5 mbar, which correspond to a region in the Jovian mesosphere. The measurements suggest that these layers, which are also seen in Voyager 2 data, are global in nature. Because these layers have a moderate opacity, further analysis of their structure and local properties will be important in analyzing spectroscopic observations of Jupiter, and indeed may provide information on the circulation of the upper atmosphere.

Dark-side observations. Voyager 1 observations of the dark side of Jupiter revealed several lightning flashes at high

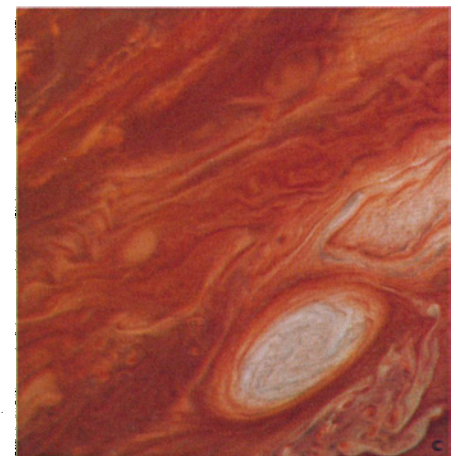
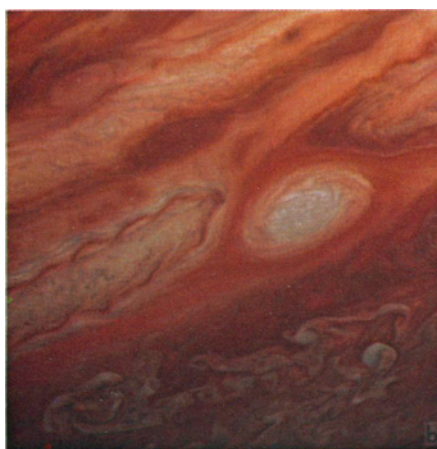


Fig. 6. High-resolution pictures of the major long-lived spots in the Jovian atmosphere, illustrating their morphological similarities. (a) The GRS and the oval just to its south on rotation 442 (7 July 1979). (b and c) The other two ovals (features 1 and 9, respectively, in Fig. 1) on rotation 440 (6 July). The area in (a) is about 36,000 km wide; (b) and (c) enclose areas about 24,000 km on a side. These images were prepared by G. W. Garneau at the JPL Image Processing Laboratory.

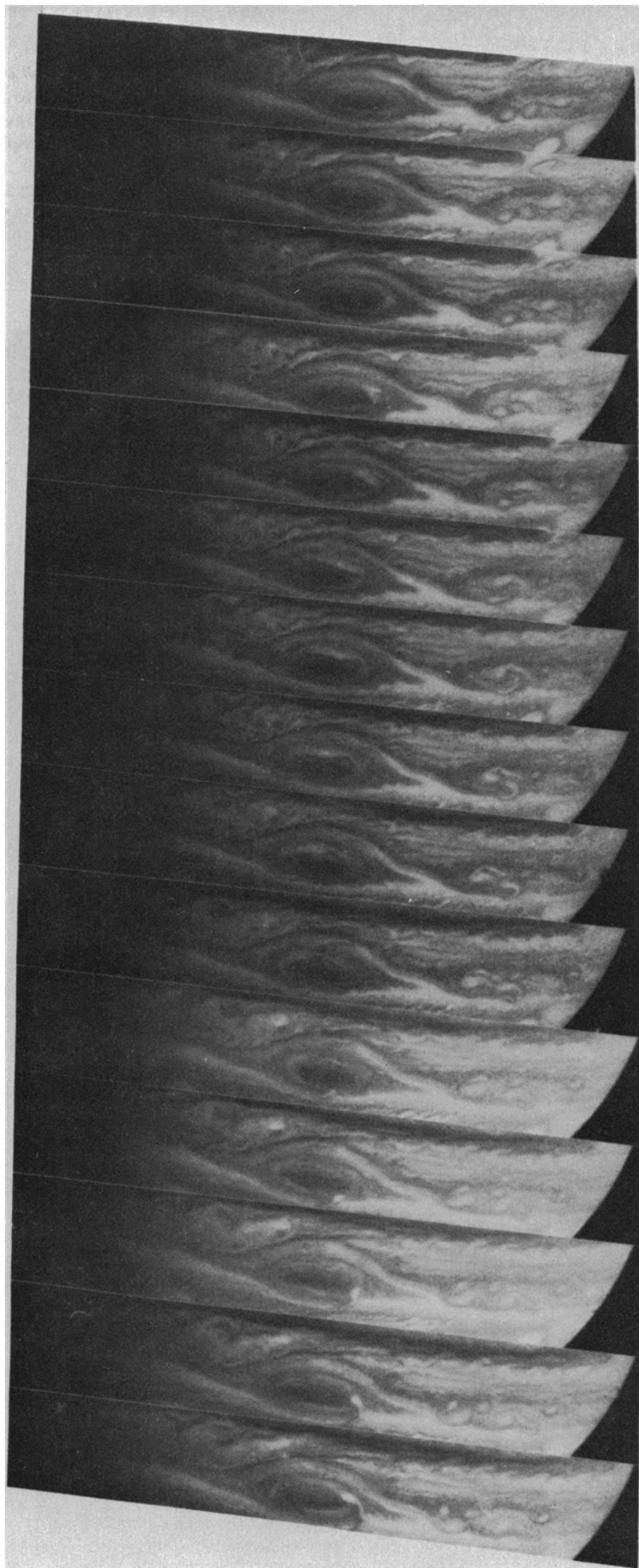


Fig. 7. Time-lapse sequence of pictures showing the flow in the neighborhood of the GRS. The time between each strip of the drift chart is 10 hours (one Jovian rotation). The major change in the flow to the east of the GRS is clearly seen. Small cloud vortices are evidently moving toward the GRS and are then deflected southward into an eastward current. At one stage as many as five small cloud vortices are apparent in the flow. Throughout the interval shown here, the GRS rotates in an almost undisturbed manner. A small interaction in which a bright cloud develops near the southern boundary is seen in picture 12 of the sequence. Small brightenings are evident to the west of the GRS. This type of behavior is consistent with convective activity produced in the wave systems. This sequence includes rotations 311 to 325 (13 to 19 May 1979) and shows an area about 25,000 km in size from north to south.

latitude in the northern hemisphere. Similar observations of Jupiter by Voyager 2 indicate that the phenomenon is global in extent. While the spacecraft was in the shadow of Jupiter, a mosaic of the planet was made with the wide-angle camera. Six lightning flashes were detected in the violet filter and two in the orange filter. The great distance from Jupiter of the Voyager 2 flyby and the lower throughput of the filters used in the Voyager 2 sequences have resulted in the observation of fewer lightning flashes than were recorded by Voyager 1 (10).

The lightning appears in one frame as a bright point surrounded by a faint corona due to the presence of the haze layer that extends above the cloud tops. More extensive patches of lightning do occur, and in one case it would appear that a small but resolvable convective system is entirely illuminated from within by lightning.

Jupiter's ring system. After the discovery of the Jovian ring system by Voyager 1 (1), additional images were planned for Voyager 2 at various illumination and viewing angles. In particular, an effort was made to obtain pictures slightly out of the equatorial plane in order to determine the width and inner structure of the ring system. A more complete account of these results and their interpretation may be found elsewhere (11).

Two Voyager 2 pictures, taken prior to ring plane crossing when the spacecraft was 2.5° above the plane, show distinct inner and outer boundaries of the brightest part of the ring system. In them the rings were viewed in backscattered sunlight, at a time when the center of the 0.1° diameter solar disk was 0.03° below the ring plane. Although the signal was weak, no obvious gaps were visible. A second set of images was acquired during the ring plane crossing. They con-

firmed Voyager 1 observations that the ring system is optically very thin with a well-defined outer edge. Smearing caused by spacecraft motion prevented any improved definition of ring thickness; the 30-km upper limit set by Voyager 1 is still the best estimate.

The most spectacular ring pictures were obtained by Voyager 2 on 11 July at a phase angle of nearly 180° while the spacecraft was 2° below the ring plane and in the shadow of Jupiter. Strong forward scattering by ring particles gave well-exposed images that provided substantially better definition of the ring structure than had been possible earlier. Figures 9 and 10, acquired during this sequence, were taken with both the narrow- and the wide-angle cameras through the clear, violet, and orange filters.

The outer part of the ring system is made up of a relatively bright segment about 800 km wide surrounded by a somewhat dimmer and broader segment about 5200 km across. Other, less distinct divisions are barely visible in Fig. 10. The interior of the ring is filled with much fainter material, probably extending downward into the top of the atmosphere of Jupiter itself. This material may contribute to the ultraviolet absorbing haze in Jupiter's upper atmosphere if stratospheric winds could give it planet-wide distribution. It is even possible that the ring material is a source of oxygen to the upper atmosphere that could be related to the abundance of carbon monoxide (12). The discovery of this inner material reinforces an earlier suggestion (11) that much of the ring system represents a steady state between loss and supply, being neither a leftover from the original accretion and condensation events that formed the planet (as Saturn's rings may be) nor fragments of a disrupted satellite. Candidates for sources to supply this material include cometary and meteoritic debris, impact ejecta from the inner satellites, and volcanic ejecta removed from Io, possibly by magnetospheric forces. The small newly discovered satellite (13) with an orbital radius of 1.81 Jupiter radii (R_J) may provide an explanation for the location of the outer boundary of the ring system.

Satellites: Introduction. One of the principal selection criteria for the Voyager 2 trajectory was to provide observations of the Galilean satellites complementary to those made by Voyager 1 (1). This trajectory included close encounters with Callisto and Ganymede prior to Jupiter closest approach, allowing viewing of the hemispheres opposite

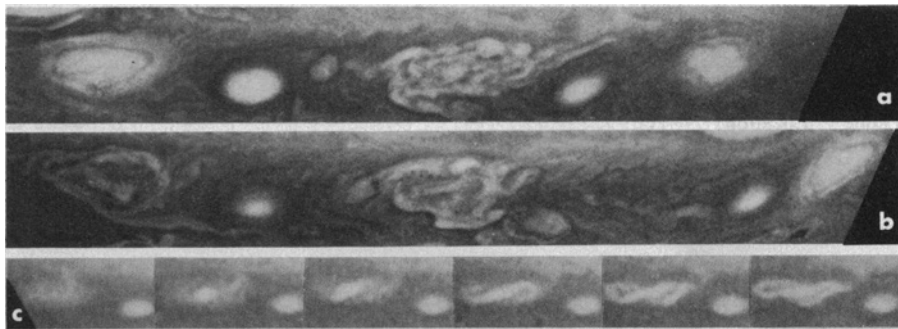


Fig. 8. (a and b) A portion of Jupiter's south polar region at two times, about 4 months apart. Part (a) was taken by Voyager 1 on rotation 119 (24 February 1979); part (b) was taken by Voyager 2, from the same range, 303 rotations later (rotation 422, 28 June). The height of each of these strips corresponds to about 10,000 km on the surface of Jupiter. Bright, cyclonic ovals with dark outlines are seen at the left (west) and right ends of (a) with a cyclonic region of folded filamentary morphology seen near the midpoint. In (b) the western oval (alone) is seen to have changed in morphology to resemble the folded filaments. The period of transformation, first noted by C. C. Avis, was observed by Voyager 2 at poorer resolution and is shown in (c). The left panel in (c) shows the subject oval as a diffuse, light gray region on rotation 287. The following panels show the same region on rotations 289 through 293; an initial small brightening at the oval's center is seen, followed by an elongation of the bright material coupled with S-shaped distortion by the spot's cyclonic rotation.

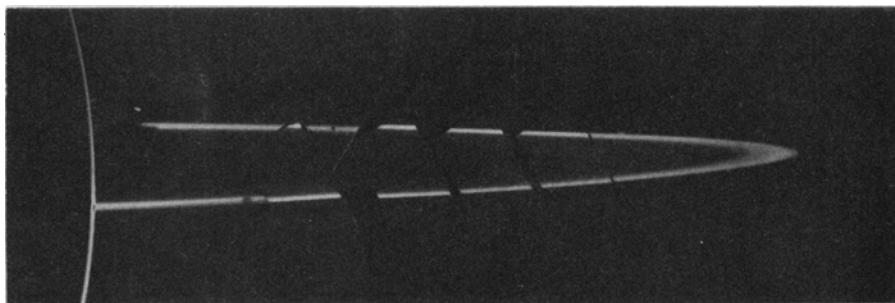


Fig. 9. This Jovian ring mosaic is comprised of two wide-angle and four narrow-angle pictures. These data were taken while the Voyager 2 spacecraft was 2° below the Jovian equatorial plane in Jupiter's shadow at a range of 1,550,000 km. Gaps between several of the images account for the discontinuities seen here. Jupiter's shadow is cast on some of the upper ring segment (the part that is closest to the spacecraft).

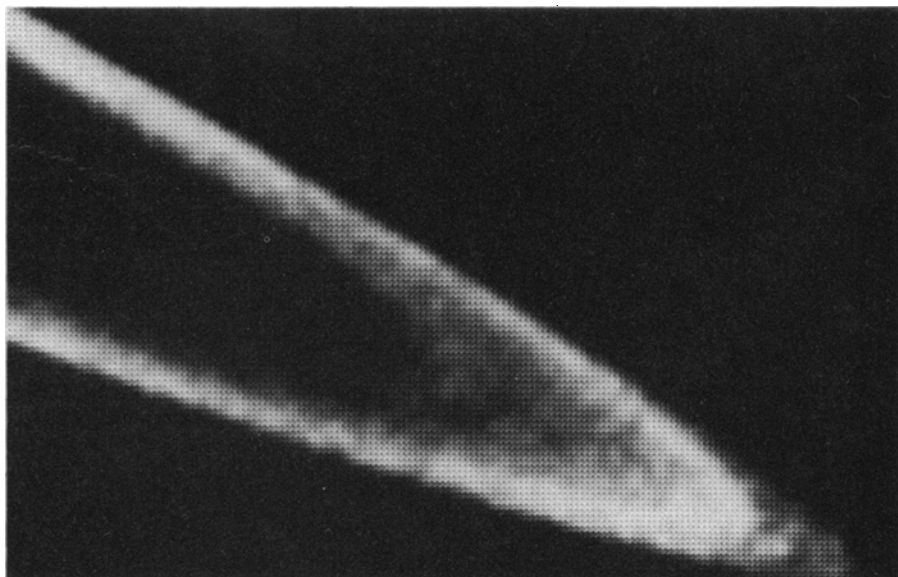


Fig. 10. Enlarged portion of a wide-angle picture taken by Voyager 2 through the clear filter, showing the brightness variations within the ring ansa: the thin brightest region and somewhat dimmer regions both interior and exterior to it. It appears that ring material may extend down to Jupiter's cloud tops. The brightest segment is approximately $1.8 R_J$ from the center of Jupiter. This picture was taken at a range of 1,556,000 km from the center of Jupiter, about 27 hours after closest approach of Voyager 2.

Table 1. Summary of Voyager 1 Io plume measurements.

Plume	Location*	N†	Time of first observation		Time of last observation		Duration		Plume width* (km)	Plume height* (km)	Central fountain width* (km)	Plume height/plume width	Plume seen by Voyager 2
			Day	Hour	Day	Hour	Day	Hour					
1	19°S, 257°W	4		-16.9	+3	1.4	3	18.3	1000 (cl)	280 (cl)	35 (uv)	0.3	
2	19°N, 305°W	8	-3	6.0	+3	1.4	6	7.4	210 (cl) 585 (uv)	100 (cl) 210 (uv)		0.5 (cl) 0.3 (uv)	X
3	3°S, 153°W	4	-1	3.8		-9.3		18.5	250 (cl)	70 (cl)	15 (cl)	0.3	X
4	21°N, 177°W	2	-1	1.6		-5.6		20.0	75 (v)	95 (v)	20 (v)	1.2	?
5	27°N, 119°W	4	-1	11.3		-11.1	1	0.2	200 (cl)	80 (cl)	?	0.4	X
6	19°N, 122°W	3	-1	9.9		-11.1		22.8	250 (cl)	80 (cl)	60 (cl)	0.3	X
7	25°S, 210°W	2		0.0		+0.5		0.5	180 (cl)	120 (cl)	?	0.6	X
8	42°S, 50°W	3		0.0		+2.0		2.0	150 (cl)	70 (cl)	15 (cl)	0.5	X

*These values are very approximate pending additional data reduction and more accurate measurements. †Each observation may be a single image or a sequence of several images taken through various filters; cl, clear filter measurement; uv, ultraviolet filter measurement; v, violet filter measurement.

those imaged by Voyager 1 at comparable resolution. A closer observation of Europa was also a major feature of the Voyager 2 encounter; the resolution was 4 km per line pair (lp) at 200,000 km on Voyager 2 compared with 33 km/lp at 1.8×10^6 km on Voyager 1. Although the Voyager 2 trajectory did not include a close encounter with Io, in response to the Voyager 1 observations (1) a special imaging sequence was added to monitor Io's active volcanic plumes and to search for new eruptions and changes in surface features since the Voyager 1 encounter.

Figure 11 illustrates the best resolution acquired by the two Voyager spacecraft as a function of longitude for each of the satellites. The full extent of coverage and approximate resolution can be seen in the global airbrush maps (Figs. 12 and 13). The maps of Europa, Ganymede, and Callisto are preliminary, uncontrolled airbrush renditions and have local errors of the order of 10° , pending further analysis and geodetic control. The base map for Io has substantially better control and should be accurate to $\sim 2^\circ$.

Among the major results of the Voyager 2 imaging experiment for the satellites are the following:

1) The entire surface of Callisto has a high density of craters several tens of kilometers or larger in diameter; no large ring structures other than the two discovered by Voyager 1 are evident in the Voyager 2 images.

2) Ganymede's surface is marked by highly complex tectonic patterns and consists of four basic terrain types: (i) dark, densely cratered terrain; (ii) grooved terrain of diverse patterns and ages; (iii) a young, rugged impact basin and ejecta blanket; and (iv) smooth terrain, which occurs in patches that locally obscure older terrains. The largest area of old cratered terrain, about 4000 km across, contains part of a giant concentric ring structure that is similar in

some respects to the giant ring structures on Callisto.

3) Europa has a smooth surface crisscrossed with highly complex fracture patterns that show little or no relief except for thin, bright ridges perhaps a few hundred meters high. Three impact craters (~ 20 km in diameter) have been identified, which suggests that the surface of Europa is relatively young compared to that of Ganymede and Callisto, but is probably at least several hundred million years old.

4) The volcanic activity on Io discovered by Voyager 1 was continuing during the Voyager 2 encounter: of seven volcanic plumes (out of eight) that were observed again, six were still erupting. The largest plume (plume 1) had ceased activity, the next largest (plume 2) had increased in size and complexity, and an additional plume was evidently active sometime during the period between the two encounters.

Amalthea. Amalthea, orbiting Jupiter between Io and the new satellite 1979J1 (13), was revealed by Voyager 1 images to be an elongated, irregular, possibly cratered body. The television observations also confirmed its very low albedo and red color. Several Voyager 2 images (resolution ~ 10 km/lp) were obtained of Amalthea in silhouette against the disk of Jupiter, providing a nearly end-on view (subspacecraft longitude $\sim 160^\circ$) of the elongated body (Fig. 14). The apparent dimensions of Amalthea in the transit frames (Fig. 14) are about 160 by 160 km. Although the polar dimensions could be in error by as much as 10 percent, owing to vidicon beam bending, the polar axis measured by a Voyager 1 image at a similar longitude (195°) is about 155 km. The current best values for Amalthea's dimensions are 270 ± 15 km (long axis), 170 ± 15 km (intermediate axis), and 155 ± 10 km (polar axis). The long axis is oriented radially with respect to Jupiter. The east-west dimension in the transit frame (Fig. 14) is actually less than our best estimate of either the long or the intermediate axis, which suggests that the body has a distinctly faceted or diamond shape.

Io. During the Voyager 1 encounter, eight volcanic eruption plumes were observed on Io over a period of $6\frac{1}{2}$ days (1, 14). Table 1 lists the plume characteristics as seen by Voyager 1 and indicates which plumes were still active during the second encounter. In an attempt to place

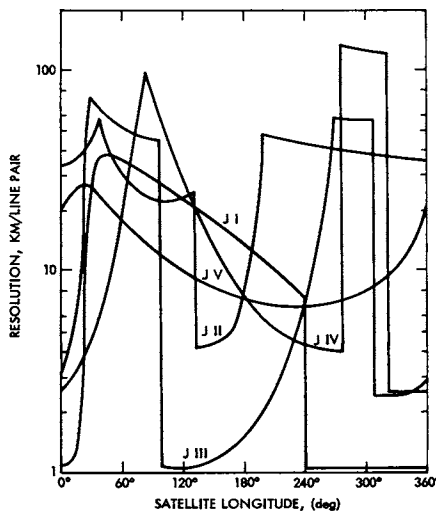


Fig. 11. Combined resolution versus satellite longitude coverage for the two Voyagers. Each of the five largest Jovian satellites (Io, J I; Europa, J II; Ganymede, J III; Callisto, J IV; and Amalthea, J V) was photographed throughout its final orbit before each Voyager's closest approach. Image resolution varies as a function of surface longitude because of the decreasing spacecraft satellite range during the satellite's orbital period. Consequently, the poorest resolution on the outer moon, Callisto, is substantially worse than the poorest Amalthea coverage. Sharp discontinuities in resolution correspond to the terminator longitudes at the times of closest satellite approach. Because the closest approaches of Voyager to Io, Ganymede, and Callisto were at high latitudes, longitudinal coverage is not completely representative.

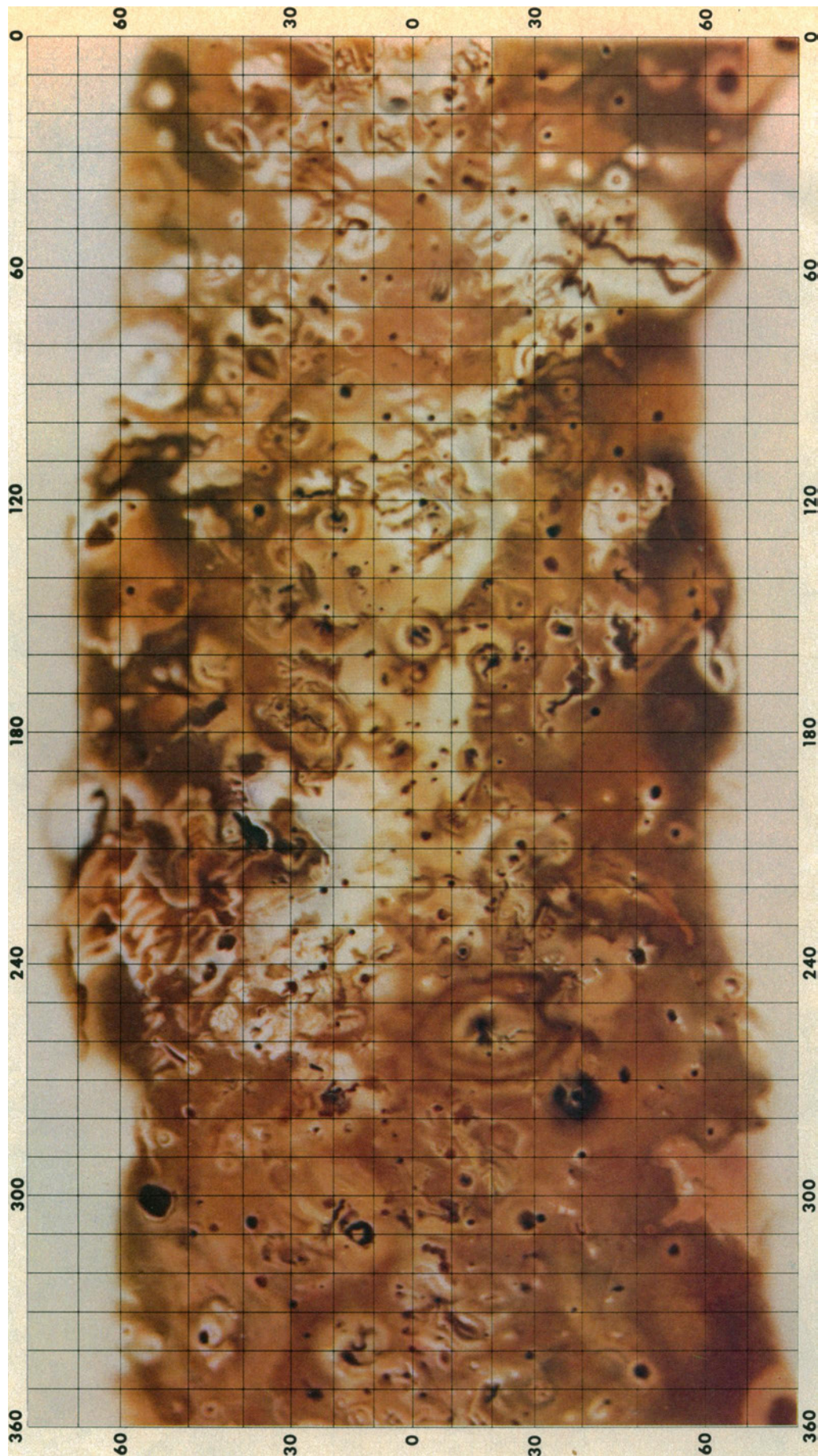
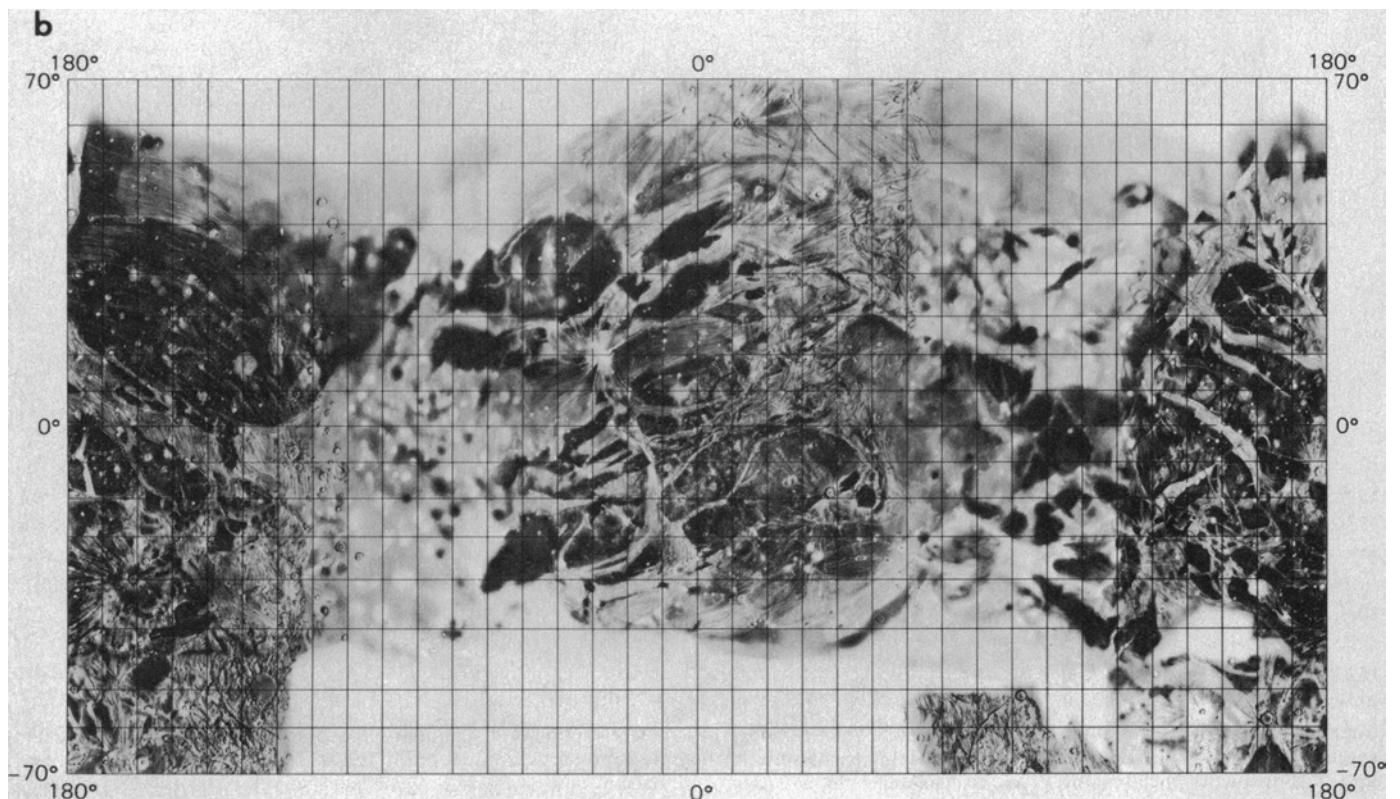
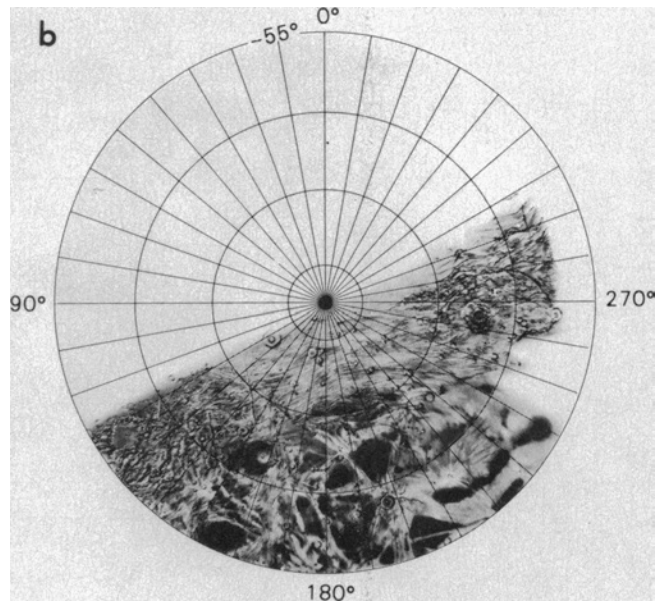
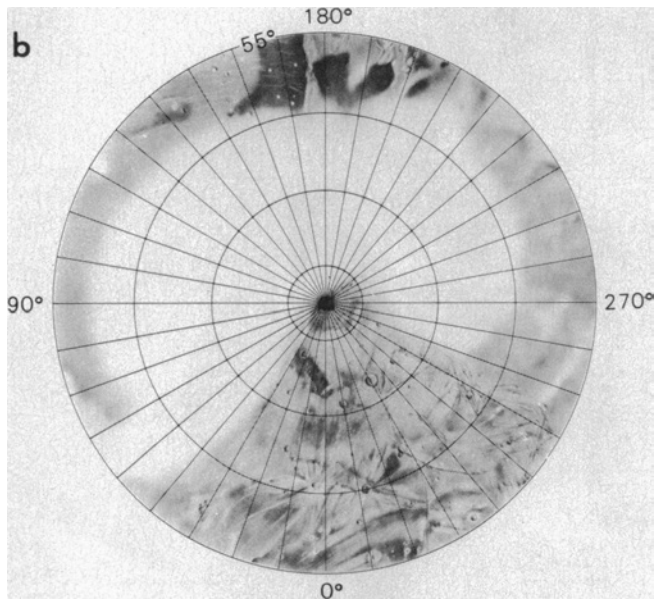
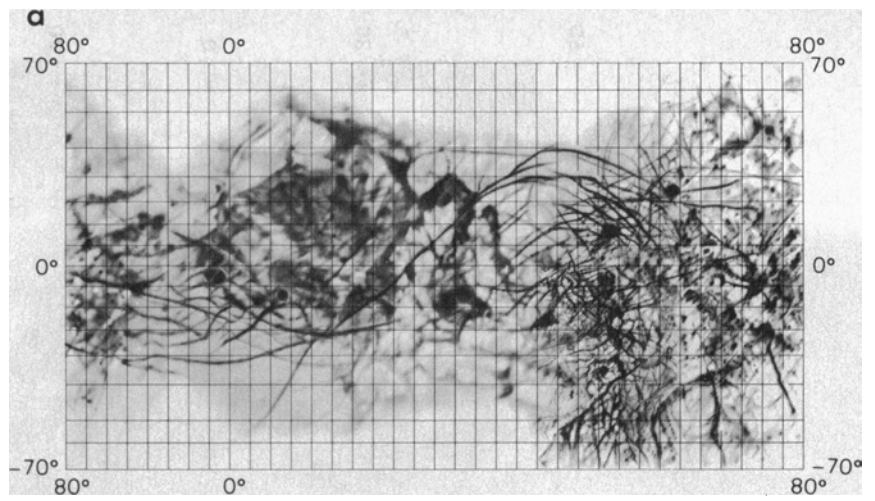
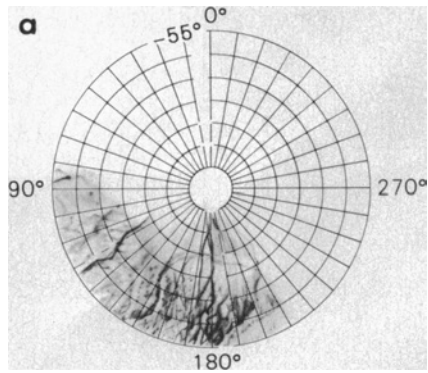


Fig. 12. Controlled shaded relief map of Io. Complete color coverage of Io at a resolution of < 20 km/lp was acquired from the Voyager 1 and 2 spacecraft. This map was assembled by using a preliminary controlled net; positions are accurate to $\sim 2^\circ$. The scale is 1:50,000,000 (1 cm = 500 km). Airbrush work was done by P. M. Bridges under the direction of R. Batson, both of the U.S. Geological Survey.



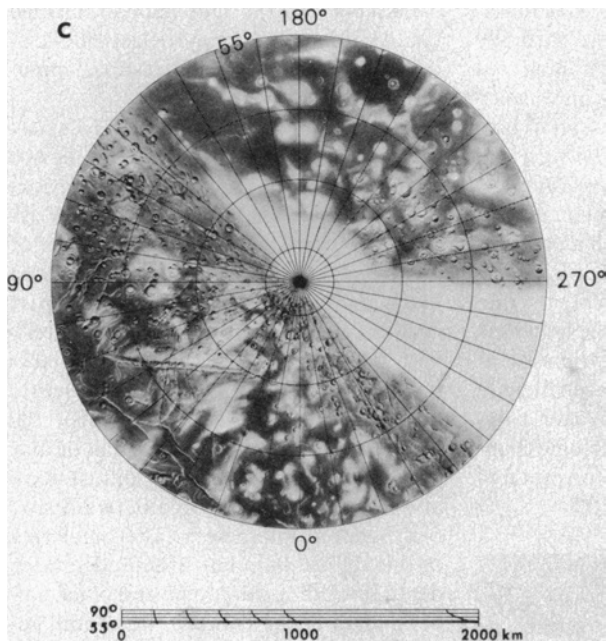
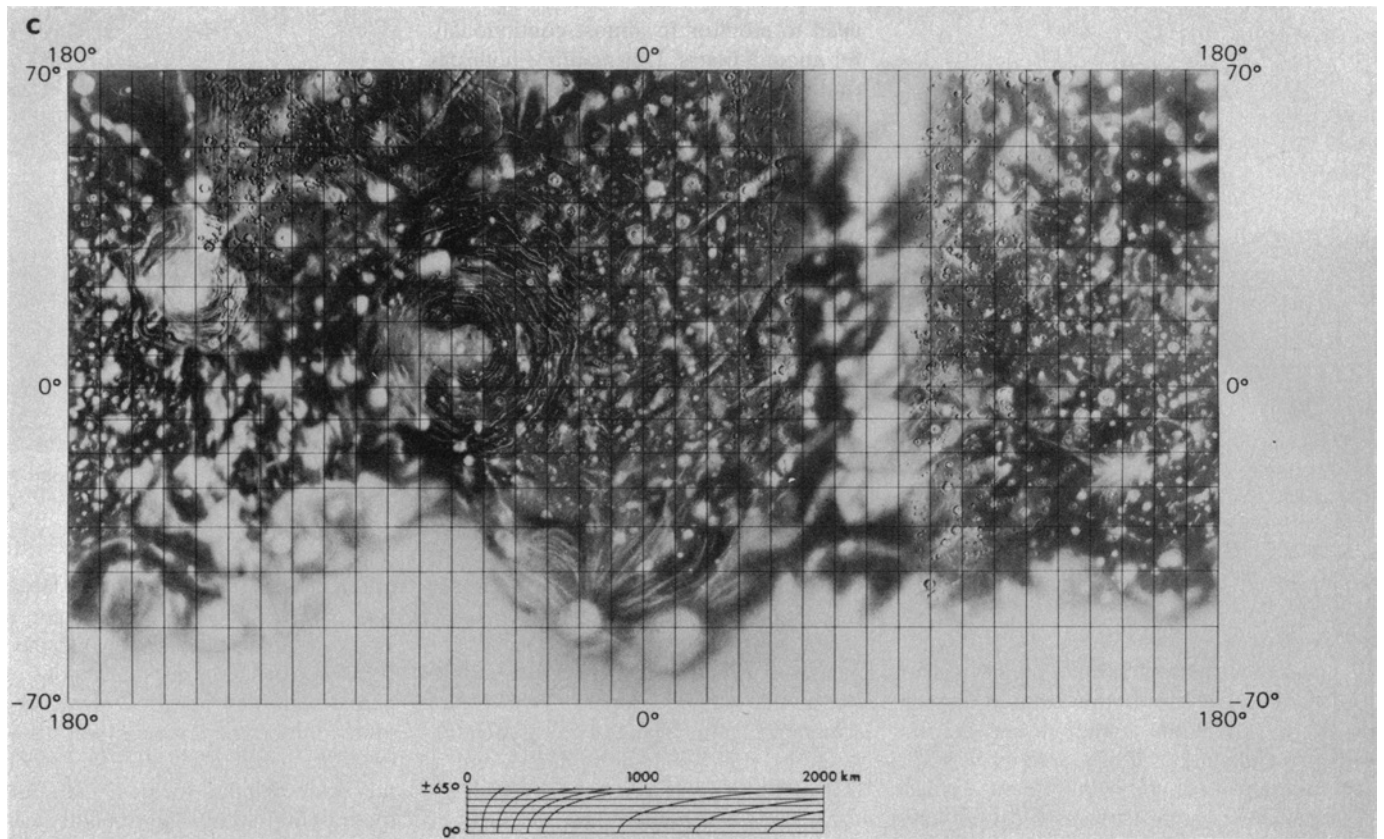


Fig. 13. Shaded relief maps of (a) Europa, (b) Ganymede, and (c) Callisto. These maps were prepared from images with a wide range of resolution. They are uncontrolled and very preliminary but are provided for orientation in the discussions that follow. The scale is 1:100,000,000 (1 cm = 1000 km); both topography and albedo are portrayed. The maps were produced by J. Inge (Europa and Ganymede) and P. M. Bridges (Callisto) under the direction of R. M. Batson, all of the U.S. Geological Survey.

limits on the extent and duration of this volcanic activity, Io was observed by the Voyager 2 television system intermittently for a 5-day period at resolutions varying between 90 and 21 km/lp; the satellite was monitored with a nearly continuous 8-hour sequence of television images at high phase angles (115° to 155°) and a resolution of ~ 20 km/lp. Plumes having heights of a few tens of kilometers can be identified with confidence only when they are within 10° of the bright

limb. Voyager 2 surveyed 80 percent of the surface in this manner, and the combined observations of Voyager 1 and 2 covered nearly 100 percent of Io. Thus all of the plumes 100 km or higher that were active during both encounters probably have been detected; in fact, most were seen several times during each encounter. Although the presence of numerous small diffuse dark spots in high-resolution Voyager 1 images suggests that relatively small eruptions

might be occurring, the fact that no active plume smaller than 70 km was seen on the limb in either encounter suggests that the large ones are far more common. Plumes 30 to 70 km high would certainly have been detectable in most of the images of the limb.

Of the eight plumes found by Voyager 1, six (plumes 2, 3, 5, 6, 7, and 8) were observed to be active during the second encounter 4 months later. The source area of plume 1 (the largest discovered

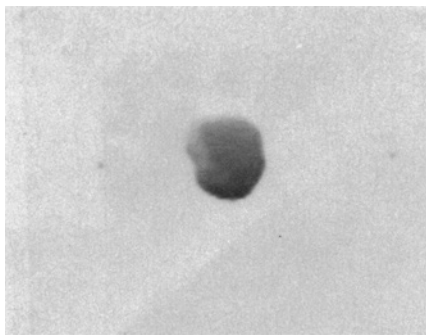


Fig. 14. Image of Amalthea in transit above Jupiter. This image was acquired at a range of 570,000 km. The anti-Jupiter face is shown (longitude on Amalthea $\sim 160^\circ$) with a phase angle of $\sim 80^\circ$. The shading in the terminator (right) and the dark rim on the bottom are due to scattered light and vidicon beam bending effects under the extreme contrast.

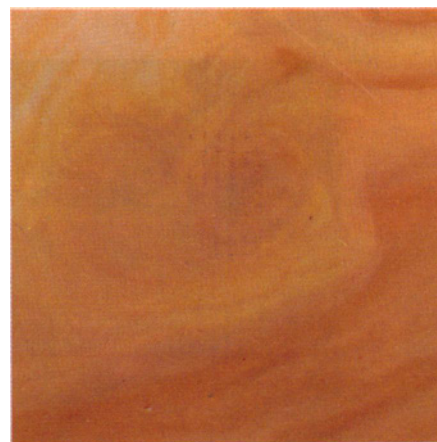
by Voyager 1) was viewed by Voyager 2 near the bright limb, but a plume was not visible. Therefore, this eruption apparently terminated sometime between the two encounters; if any activity was still taking place in July, the plume was less than 40 km high. Voyager 2 did not have the opportunity to observe plume 4, and no new active plumes were discovered during the second encounter.

Figure 15 is a comparison of plume 2 as viewed by Voyager 1 and 2 on the limb. Both pictures were taken through the clear filter and processed similarly. The dimensions of plume 2 increased between the two encounters. The Voyager 2 image apparently shows a double plume coinciding with the two ends of a 250-km-long dark feature on the surface of Io with which plume 2 is associated. During Voyager 1 encounter only the west end of the dark feature was erupting (see Fig. 18). Dimensions of the other plumes do not appear to have changed.

Figure 16 is a montage of four frames selected from the Voyager 2 image series

used to monitor Io almost continuously for about 8 hours. During this 8-hour period plumes 5 and 6 rotated into view on the bright limb, plume 8 rotated across the terminator, and plume 2 came into view when it caught the rising sun beyond the dark limb. Most (perhaps all) of the changes in the appearance of plumes 5 and 6 are due to changing viewing geometry; further study is required to determine whether actual short-term changes in the eruptions occurred during the picture sequence. All plumes appear to scatter blue and violet light more strongly in the forward than the backward direction; one possible explanation for this is that they contain particles of the order of $1 \mu\text{m}$ in diameter. Figure 17 is a color reproduction of plumes 5 and 6 from one of the last frames in the Io sequence.

Several large-scale changes in the appearance of Io's surface occurred between the two encounters. Two of the more prominent changes are associated with the regions near plumes 1 and 2 (Figs. 18 and 19). During the 4-month interval between encounters, the cleft in the southern area of the heart-shaped dark ring associated with plume 1 was filled in by darker material. The markings near the central vent are virtually unchanged, however, demonstrating that they are true albedo features on the surface and not plume material seen in projection against the surface. The west end of a black strip at plume 2 (possibly a fissure) on the second-encounter picture shows a broad white ring with a dark diffuse central core (Fig. 19) that is not as prominent as on the first encounter picture. Furthermore, much of the light area north and east of the black strip seen at the first encounter has since been filled in with darker material. On Voyager 1 images, most of the activity of plume 2 appeared to be associated with the east end



Mosaic of Voyager 2 images of cloud structures, with more nearly natural color.

of the black strip. Four months later, the west end seemed to have become more active, perhaps accounting for the two components and larger dimensions of the plume seen by Voyager 2 (Fig. 15). Another important change was the increased albedo of the northern part of the black annulus located just south of the eruption sites. The annulus was observed by the infrared interferometer (IRIS) on Voyager 1 to be a prominent "hot spot" (15). This albedo change could be the result of pyroclastic deposition from plume 2 over part of the annulus.

Yet another major change in Io's surface occurred in a large area, about 600 km in diameter, northwest of plume 2, centered near 340°W , 45°N . During Voyager 1 encounter, the southern part of this region contained a variety of isolated black and orange spots. The central part now shows a complex of bright areas with a few orange and dark diffuse markings (Fig. 19a). The Voyager 2 picture (Fig. 19b) shows a large dark spot ~ 100 km in diameter (formerly a small diffuse dark region) surrounded by diffuse dark and bright rings extending outward several hundred kilometers. The outer ring of this diffuse halo has obscured surface detail, including an orange and black caldera south of the center. The overall geometry of this pattern is similar to that around active plumes, in particular plume 1. Although these changes could be due to differences in viewing geometry and lighting, it is more likely that they are due to a major eruption comparable in size to plumes 1 and 2, which began during the 4 months between the two encounters. The dark center of this ring pattern was not viewed near the limb by Voyager 2, so it is possible that this eruption was active, but not observed, during the Voyager 2 encounter.

Europa. The most distinguishing char-

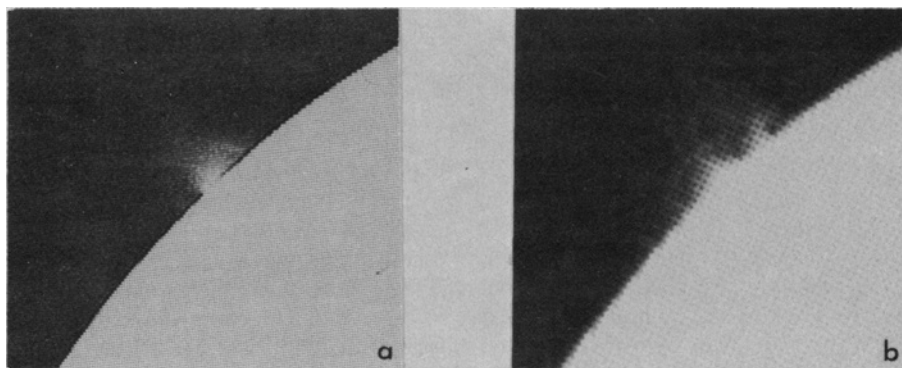


Fig. 15. Comparison of images by Voyager 1 and 2 of volcanic eruptions of plume 2. Whereas most of the plumes discovered by Voyager 1 were found to be about the same size 4 months later during the Voyager 2 encounter, plume 2 increased in height from about 120 km in the Voyager 1 image (a) to about 175 km in the Voyager 2 image (b). Plume 2 also changed in complexity from a single to a double column.

acteristic of Europa as viewed by Voyager 1 was a set of linear bands that appear to trace small and great circles transecting one another throughout the equatorial region (*l*). Whereas the limiting resolution of the Voyager 1 imaging was 33 km/lp, Voyager 2 acquired coverage of most of the region between longitudes 80° and 180°W at resolutions of ~ 4 km/lp. From Voyager 2 coverage we now see that the surface of the satellite consists of two types of terrain: (i) slightly dark mottled terrain and (ii) uniformly bright terrain crossed by numerous dark linear markings and narrow bright ridges that form cusped patterns (Figs. 20 and 21).

With images acquired several hours apart, it is possible to examine dark mottled terrain in the equatorial region and bright terrain at higher latitudes both at a high sun angle (Fig. 20) and near the terminator (Fig. 21). The mottled terrain appears rougher than the uniformly bright terrain when viewed at the terminator (Fig. 21). Numerous vague circular features a few kilometers in diameter may be craters just at the threshold of resolution. If so, craters in this size range are relatively common. The smooth bright terrain shows little contrast except for the dark lines and numerous dark spots, most of them smaller than 10 km, which appear to be distributed randomly, typically several tens of kilometers apart. In addition, there are a few discrete, irregular dark patches as much as 150 km across (Fig. 20).

The global dark linear markings seen by Voyager 1 are predominantly albedo features that have very little or no vertical relief. Although the broad linear markings are darker than the terrain they transect, their albedo is actually relatively high; the contrast between the bright and dark materials is only about 10 percent. The dark bands range in width from several kilometers to approximately 70 km. Many trace great and small circles. Some of the broader bands have a narrow bright band running down their centers (Fig. 20). In rare cases whole sections of bands are brighter than the surroundings. Although the very long bands tend to intersect at relatively small angles, in some areas the pattern is clearly reticulate with many of the bands intersecting at large angles—for example, at 10°S, 108°W, and in the region antipodal to the sub-Jupiter point. In the reticulate areas many of the bands are curved, but more generally they tend to be relatively straight. The dark bands tend to disappear close to the terminator, indicating that they have little relief, possibly less than a few tens of meters.

Along much of the length of the terminator, a totally different type of feature is observed, most frequently in the bright terrain. Numerous narrow linear ridges are superimposed on one another and on the traces of the dark linear markings visible at higher sun angles. The general impression is of strand upon strand, similar to the surface of a ball of string (Fig. 21). These ridges have very regular widths of ~ 10 km, and their visibility beyond the terminator suggests that they may be as high as a few hundred meters. In plan they vary from linear to a periodic cusped pattern much like the function $|\sin \alpha|$, where α is variable from ridge to ridge. At higher illumination angles, away from the terminator, discrimination of the ridges tends to be lost, but some are still discernible as faint bright lines. Evidently their albedo is very close to that of the bright regions in general.

Only three probable craters have been identified on Europa; all are approximately 20 km in diameter, one at

60°S, 150°W, another on the equator at 180°W, and a third near the equator at 80°W (Fig. 20). Assuming the area viewed is typical of the entire planet, there is approximately one crater larger than 20 km per 10^6 km². One of the craters near the terminator (Fig. 20) resembles a ringed impact structure superimposed on some of the bright, raised ridges and apparently raised above the surrounding terrain. The central depression is about 20 km in diameter, the second ring about 40 km, and a possible outer ring about 60 km. If this structure is of impact origin, then the appearance of the feature suggests that it has been modified by surface erosion processes or internal isostatic adjustments.

Europa's size, density, and surface photometric properties provide important clues to its bulk composition and evolution. Somewhat smaller than the moon, Europa (radius, 1565 km) has a density of 3 g/cm³ (*l*), suggesting a primarily silicate bulk composition with a small admixture of lighter materials. In-

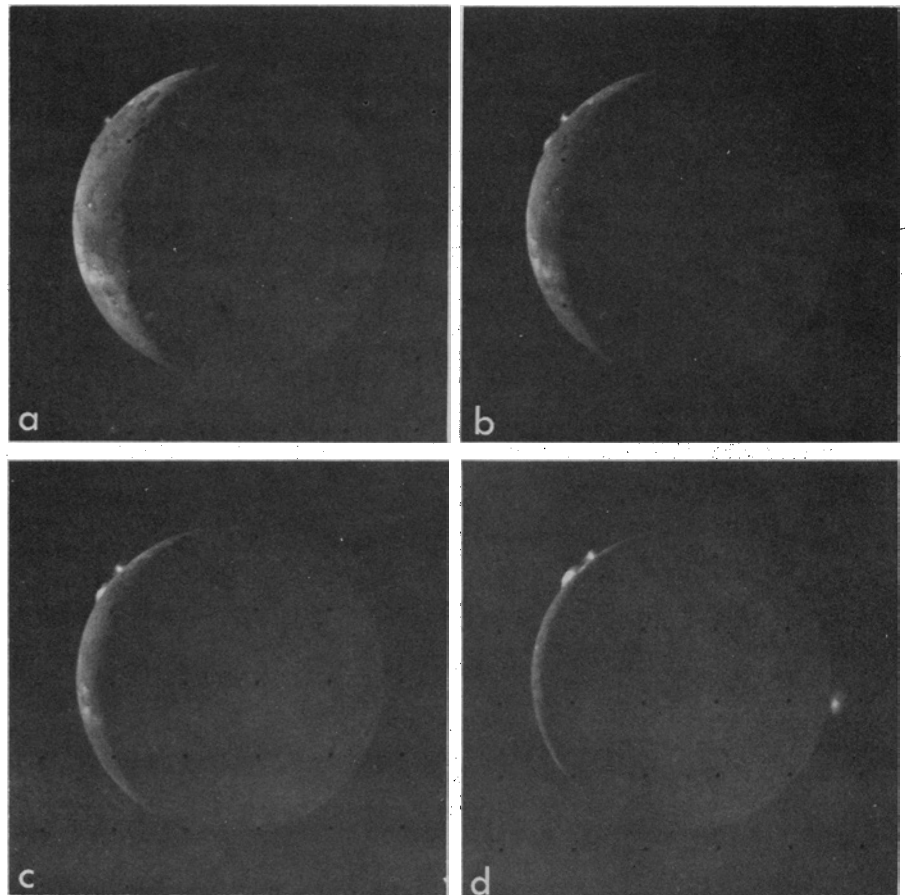


Fig. 16. Time-lapse sequence of images of volcanic eruptions on Io. These four frames are clear-filter images of Io acquired by Voyager 2 during an 8-hour sequence in which the satellite was imaged nearly continuously at a range of about 10° km at phase angles between 130° and 160°. These images show plumes 5 and 6 as they rotate onto the west limb, plume 8 as it vanishes on the evening terminator, and plume 2, visible to a height of 250 km, as it emerges in the morning sunlight (east limb) at the end of the sequence. The apparent brightening of plumes 5 and 6 is real as the phase angle approaches 160°, suggesting strong forward scattering of small micrometer-size particles (probably fine condensate, perhaps SO₂).

frared spectra and the observed high albedo indicate that much of Europa's surface is covered with water ice or frost (16). A simple model for Europa is a predominantly silicate body with a thin layer of ice or water. The thickness of water implied by the bulk density depends on the assumed mean density of the silicate part. Previous models have used water-ice thicknesses ranging from ~ 75 km (17) to ~ 150 km (18). For example, using the current best values for radius and density (1) and assuming that all the water is now in the outer layer, the thickness of a water layer would be ~ 80 km for lunar-density silicate (3.34 g/cm³) to ~ 120 km for silicate (+ Fe or FeS) with Io's bulk density (3.5 g/cm³).

The present state of the water layer depends on the details of Europa's thermal evolution. Radiogenic heat production from chondritic abundances of radionuclides in the silicate fraction would yield a present-day energy flux of ~ 7 erg/cm²-sec (19). Models assuming conductive heat transport result in a solid ice crust ~ 40 to 50 km thick overlying liquid water. This thickness is about half that obtained for the solid ice crust of Ganymede from similar calculations (17, 18), because the estimated surface flux of radiogenic energy is higher on Europa (20). If solid-state convection in ice is an important mechanism of heat transfer, the liquid water mantles of Europa, Ganymede, and Callisto can all be frozen in short periods of time (< 10⁹ years); in this case there will be a stiff, thermally conducting crust of similar thickness overlying a softer convecting layer of ice (19, 20). Tidal heating is not of sufficient magnitude to melt a completely frozen water layer on Europa, but might have prevented original freezing of a water mantle if the tidal resonances were established early enough (19). One of the possible consequences of such models is that large-scale topographic relief (linear dimensions of 75 to 100 km or greater) probably collapses more readily by cold viscous flow in the ice crust on Europa than on Ganymede and Callisto (17, 18). The apparent absence of mountains or large craters may thus be partially due to the effects of cold flow in a fairly thin, stiff crust (21).

Analysis of the Voyager 2 images provides possible clues to the thickness of the water layer. The presence of at least two terrain types, one darker and rougher, one brighter and containing the dark linear markings, suggests some lateral variation in properties or processes that may be related to the underlying silicate core of Europa. For instance, the mot-

ted terrain may represent areas where the silicate core is close (within ~ 10 km) to the surface of the ice. If this is the case, the total water thickness must be less than that implied by the models discussed above (< ~ 50 km) or topography on the silicate surface is extraordinarily great for a body of Europa's dimensions (17, 18). A water layer this thin would imply a density for the silicate fraction below 3.3 g/cm³. One simple explanation for this situation would be that the silicate core of Europa still contains significant amounts of volatiles, primarily water.

This preliminary analysis suggests a possible scenario for Europa's history as follows. (i) An early liquid water "ocean" (with thin ice crust) covered the satellite, either contemporaneous

with or immediately following the end of the final accretional bombardment. This ocean obliterated or covered the ancient heavily cratered surface. (ii) Continual freezing of the liquid layer resulted in large-scale expansion of the crust, producing fracture patterns, filled with fluids from below, now visible as dark markings. (iii) A stable ice crust thick enough to preserve craters formed at a period somewhat later than Ganymede's grooved terrains; this crust has retained only a record of relatively recent, low-intensity postaccretional bombardment.

If the dark markings are, in fact, the expression of crustal expansion due to freezing of an early ocean, the amount of expansion implied is about 5 to 15 percent of the surface area (based on estimates of stripe widths in the Voyager 2 images). Cassen *et al.* (19) calculate that volume expansion during freezing of a 100-km-thick layer of water would be only about 1 percent. This model, however, assumes that a preexisting liquid layer freezes uniformly. If, instead, a thin (~ 50 km) ocean were produced over a period of time by outgassing of water from the interior, a frozen crust continually adjusting to the increased volume of the ocean could show a greater increase in area (~ 5 to 10 percent).

Another process that may have affected Europa's surface over geologic time is sputtering by charged particles, particularly positive ions. Sputtering has been suggested as a possible mechanism for removing atoms from Io (22), and recent laboratory work suggests that yields for water ice sputtering are much greater than those for rock materials (23). Lanzerotti *et al.* (24) have suggested that sputtering yields on Europa could be of the order of 10⁸ to 10¹¹ molecules per square centimeter per second. Their estimate was based on proton yields and Pioneer 10 energetic particle data and Earth-based observations of sulfur. Voyager 1 and Voyager 2 results suggest that a significant proportion of the positive ions may be heavy ions (that is, sulfur and oxygen), which would have even greater yields than protons. Thus, significant amounts of erosion may have occurred on Europa over geologic time, equivalent to tens of meters to kilometers. The pedestal crater seen near the terminator (Fig. 21) superposed on the cusped ridges and standing above the surrounding surface may be evidence for such erosion.

Ganymede. Voyager 2 encountered Ganymede before Jupiter, viewing at high resolution the anti-Jupiter hemisphere (central longitude ~ 180°), thus

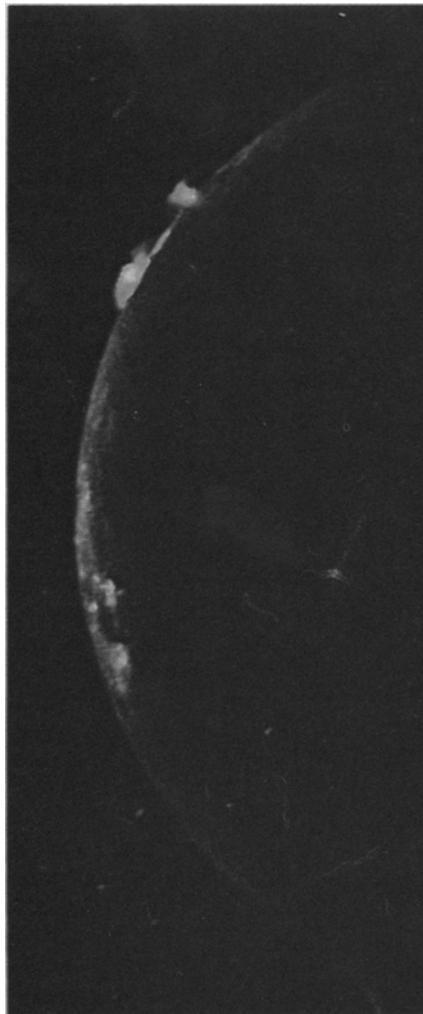


Fig. 17. Voyager 2 acquired this picture of Io on 9 July 1979, from a range of 1,200,000 km. Two volcanic eruption plumes that are about 100 km high and strongly scatter in blue light are seen on the limb. These two plumes were first seen by Voyager 1 in March 1979 and are designated plume 5 (upper) and plume 6 (lower). They apparently have been erupting continuously for more than 4 months.

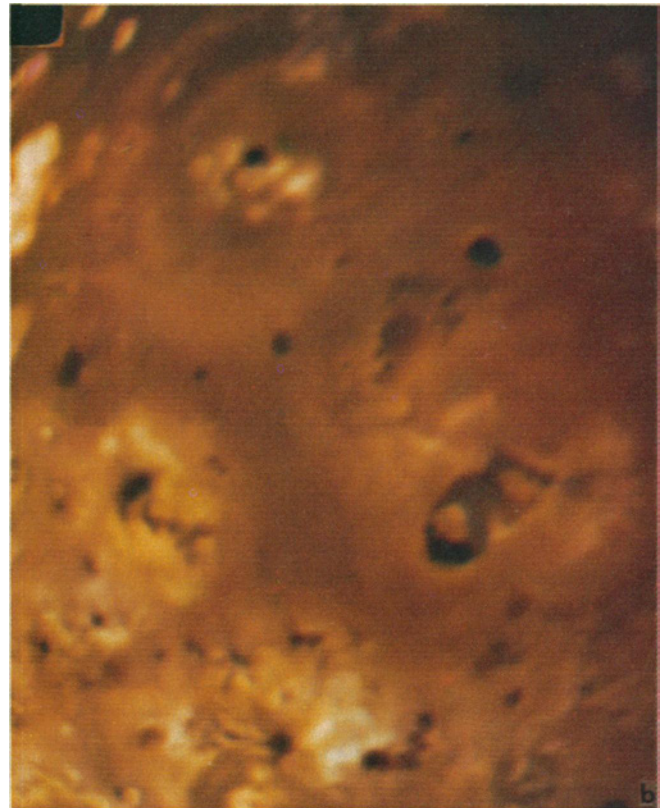
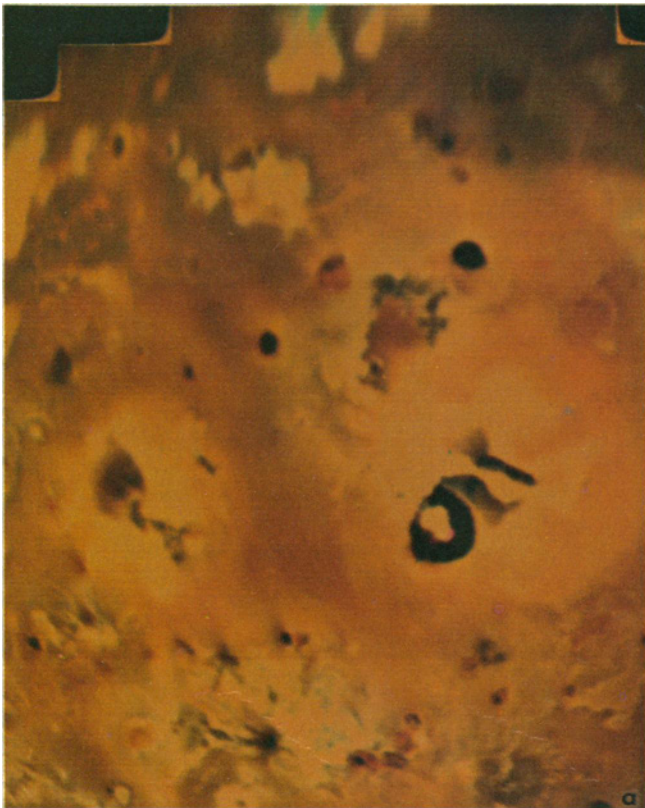
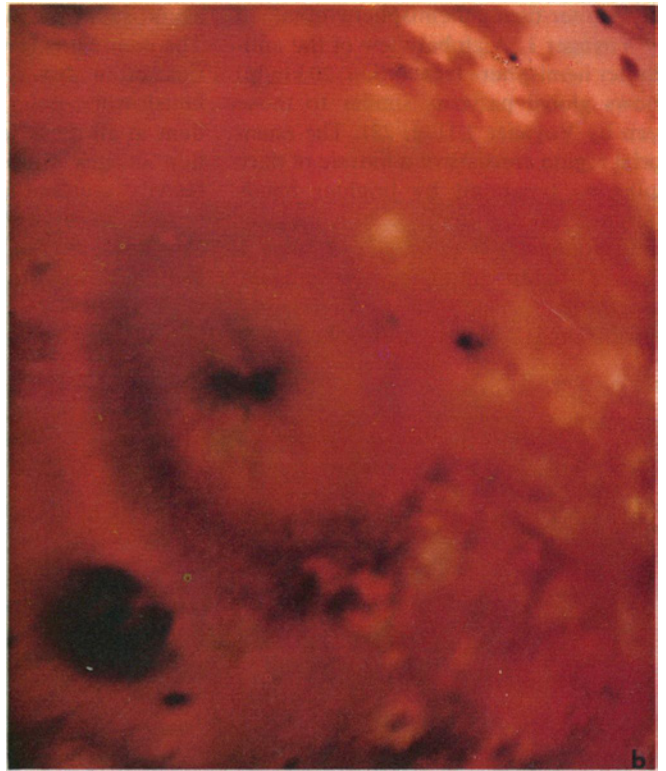


Fig. 18 (top). Comparison of surface deposits from a volcanic plume as seen in the Voyager 1 and 2 encounters. The deposits associated with plume 1, which were seen by Voyager 1 as a concentric heart-shaped pattern of color rings (a), were found by Voyager 2 to have changed to an oval form (b). Not only had the fallout pattern changed, but plume 1, the largest seen by Voyager 1, was also found to be extinct when Voyager 2 arrived 4 months later. The heart and oval patterns measure about 1500 by 700 km. These color images were assembled from violet, blue, and orange narrow-angle frames. Fig. 19 (bottom). Changes in albedo and color on the surface of Io around plume 2 between (a) Voyager 1 and (b) Voyager 2. Plume 2 (located at $\sim 305^{\circ}\text{W}$, 18°N ; Fig. 12) changed in size and shape, as shown in Fig. 15, and the fallout pattern around it also changed between the encounters of Voyager 1 and 2. Bright patches developed near the vent of plume 2, masking older patterns. Another major change, centered north of plume 2 (near 335°W , 45°N ; Fig. 12), was the development by the time of the Voyager 2 encounter of a large concentric ring ~ 1000 km in diameter. As discussed in the text, this ring resembles the fallout pattern around plume 1, and its sudden appearance on Io suggests that a new plume developed between the two encounters. The color shown here differs from that in Fig. 18, as blue, green, and orange wide-angle images were used here for Voyager 1 and clear, violet, and blue narrow-angle images for Voyager 2.

complementing the excellent coverage of the Jupiter-facing hemisphere obtained by Voyager 1. A global view of the anti-Jupiter hemisphere (resolution, 20 km/lp) shows global patterns similar to those seen by Voyager 1 (Fig. 22). The equatorial region consists of a mosaic of dark polygons separated by brighter bands (grooved terrain), across which are scattered numerous bright-rayed craters. A general brightening in the polar regions in this view is also visible on numerous far-encounter images with resolutions of

20 to 60 km/lp acquired by both Voyagers; see, for example, figure 12 in (1). The contrast is low and the cap boundaries often fuzzy and ill-defined, but bluish-white polar caps are clearly evident in all these images. Higher resolution images show that both the dark heavily cratered and brighter grooved terrains exist in the polar regions; the caps are thus likely to be surficial deposits. The low-latitude edges of the polar caps in both hemispheres are generally between 40° and 45°. There is no appar-

ent brightness gradient toward the poles within the caps, although possible variations near the poles are obscured by foreshortening at very high latitudes. The polar cap boundaries are diffuse on images at closer range; the possible frost deposit does not visibly obscure topography at high resolution. The possibility of slow migration of volatiles on the surface toward high latitudes on Ganymede has been considered (25). That model, based on the evaporation and ballistic flight of water molecules, suggests that the ice

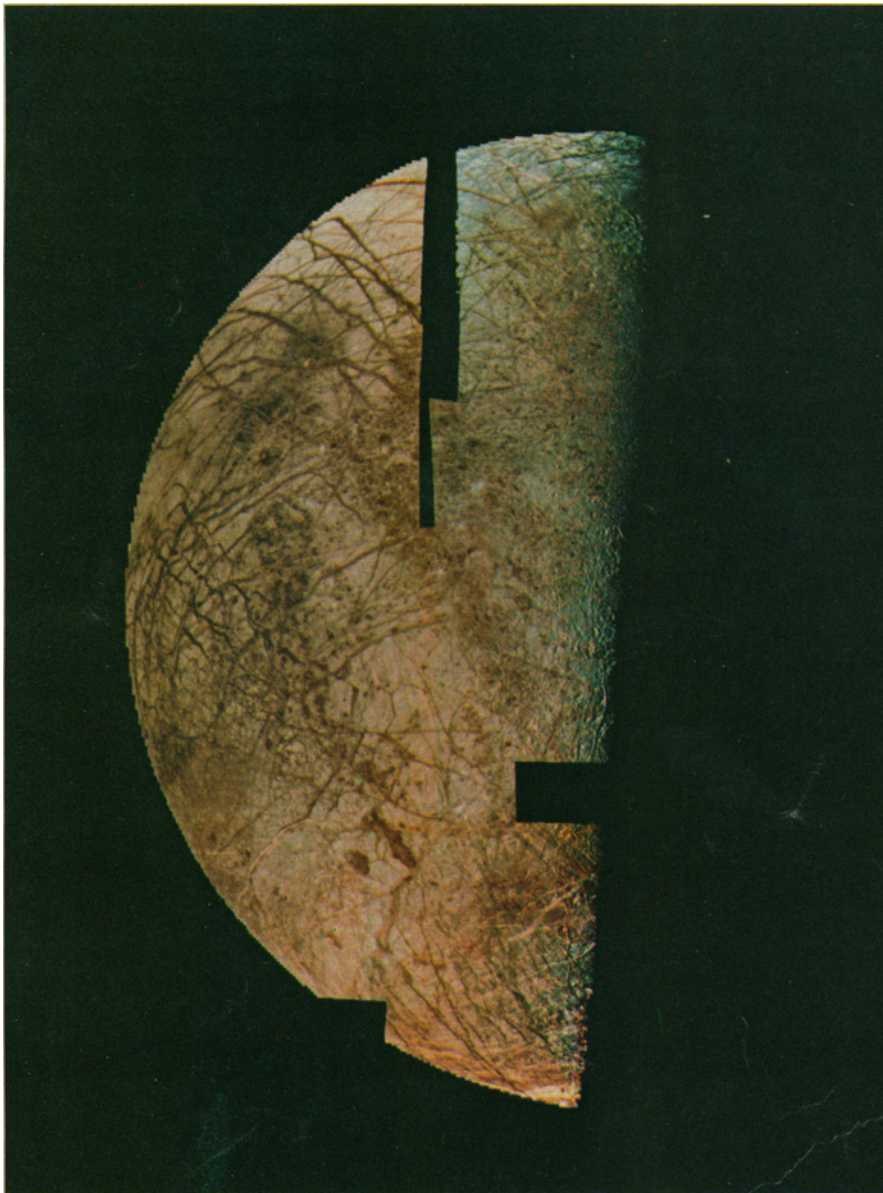
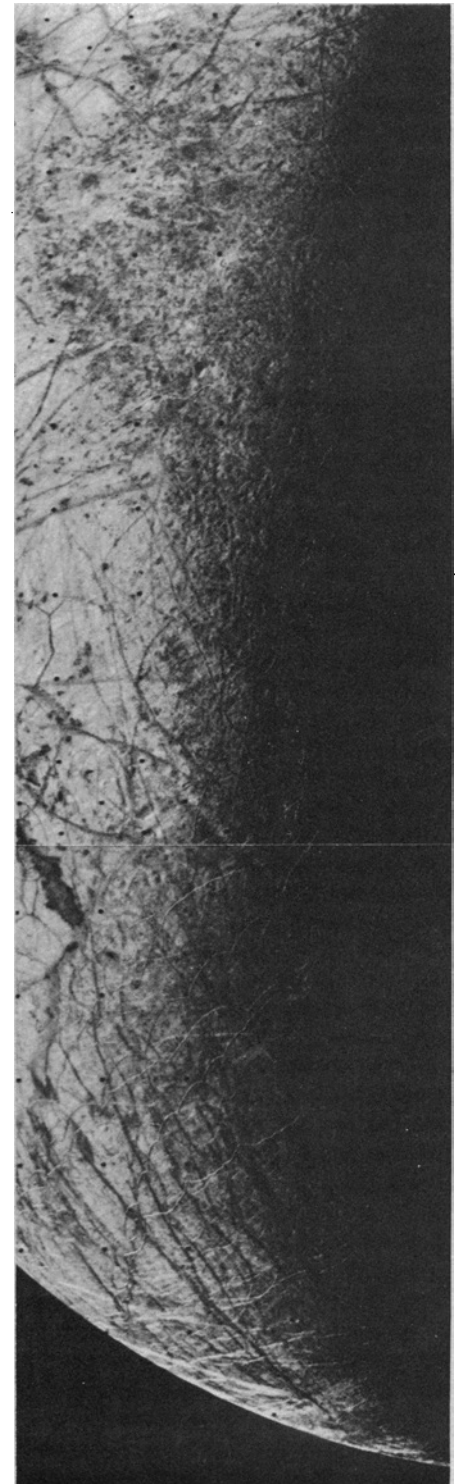


Fig. 20 (left). Computer-generated mosaic of Europa. Five sets of narrow-angle images acquired in each of three filters (violet, blue, and orange) were mosaicked to produce this image. The stair-step pattern on the limb resulted from the application of a simple photometric function ($\cos i$) to reduce limb-to-terminator contrast. A transformation was required to produce the mosaic because the images were taken from different subspacecraft longitudes as the spacecraft rapidly flew by. This mosaic was prepared by C. C. Avis at the JPL Image Processing Laboratory. Fig. 21 (right). Two-frame mosaic of Europa showing the terminator at about 150°W. Best resolution is about 4 km/lp. The terminator has moved about 15° to the west between Fig. 20 and this view. Along the northern part of the terminator is a large region of mottled terrain, which appears rougher than the surroundings and lacks dark stripes. In the southern part, numerous examples of arcuate ridges and one of the low-relief dark stripes typical of the bright terrain can be seen.



would be relatively stable at temperate latitudes (more than 30° from the equator); the apparent low-latitude boundary of the observed caps is consistent with this calculation.

In a computer mosaic showing in greater detail the regional geologic units of the anti-Jupiter hemisphere, the basic relations and units are similar to those found by Voyager 1 on the sub-Jupiter hemisphere (Fig. 23). Irregular polygons of dark, heavily cratered terrain are separated by extensive lighter bands that form segmented, branching, quasi-linear patterns. These polygonal dark areas are the most ancient parts of the crust. Where seen at high resolution by Voyager 1, the younger brighter bands were found to be composed of long parallel grooves and ridges either in parallel arrays or with intricate crosscutting relations (1). Voyager 2 has shown the grooved terrain to have much greater diversity in form, scale, and age than was previously thought.

Superimposed on both the ancient cratered terrain and the grooved terrain are younger rayed impact craters. The youngest major feature seen in the global and regional views (Figs. 22 and 23) is the largest of these bright-rayed craters, shown in Fig. 24. Its complex of rays and clusters of secondary impact craters have exposed fresh, bright materials, most likely water ice, and extend for nearly 1000 km from the primary crater.

The largest polygon of dark heavily cratered terrain on Ganymede occurs in the anti-Jupiter hemisphere, stretching from the equator to 45°N between longitudes 90° and 180° (Figs. 13b, 22, and 23). This dark area was seen in the Pioneer 10 images of Ganymede and in drawings by visual observers (2). It is the only surface feature of the Galilean satellites, except for the dark polar caps of Io, that can be easily identified by Earth-based instruments. One of the most striking discoveries of Voyager 2 is a gigantic system of bright, slightly curved, parallel streaks that sweep across this large region (Figs. 22 and 23). These markings can be seen faintly, extending across other sections of the dark terrain south and west of the large dark region. They markedly resemble the outermost sections of the large concentric ring systems on Callisto [see figure 22 in (1)] thought to have resulted from a major impact into Callisto's early soft icy crust. The center of the Ganymede ring system is near 30°S, 180°W. No central bright patch is found at this location as in the case of the Callisto ring systems; evidently formation of younger grooved terrains and impact craters has erased it.

Fig. 22. Voyager 2 color image of Ganymede taken from a range of 1,200,000 km. The image shows a large dark circular feature about 3200 km in diameter with narrow, closely spaced light bands traversing its surface. The light branching bands are grooved terrain, first seen on Voyager 1, and are younger than the more heavily cratered dark regions. The bright region above the dark circular feature is the north polar cap.



Seen at high resolution (Fig. 25) where they cross the largest section of dark cratered terrain near the equator at 130°W, the bright markings of the ring pattern are found to consist of rimmed furrows highlighted by bright material. Typical furrows are about 10 km wide, hundreds of kilometers long, probably a few hundred meters deep, and have raised rims standing about 100 m above the surrounding terrain. The furrows are spaced, on average, about 50 km apart. In detail, the course of the furrows is highly irregular, with local sharp kinks or bends. This major system of furrows can readily be traced across three large polygons of cratered terrain and probably extends farther. An apparent remnant of a second rimmed furrow system occurs on parts of the sub-Jupiter hemisphere as well, faintly visible in Voyager 1 images.

Although these furrow systems on Ganymede appear to be remnants of gigantic ring structures similar to those inferred to have been formed by ancient basin-scale impacts on Callisto, there are important differences. Individual rings on Callisto have similar planimetric form but are flat-topped ridges; had the interiors of the rimmed furrows on Ganymede been filled after formation, they might resemble the ridges on Callisto. In addition, almost all of the craters in the dark cratered terrain on Ganymede (Fig. 25) are younger than the Ganymede ring structures; only about a third of the craters found within the largest ring system on Callisto are younger than the ring structure. These differences may reflect variations in the detailed histories of the two bodies, including, for example, the

strengths of their early crusts, their cooling and freezing histories, and the availability of extrudable fluids.

More specific information on the early state of Ganymede's crust and changes in its rigidity with depth and time can be obtained from inspection of the varied morphology of craters of different ages superposed on the ancient cratered terrain. A dozen or so bright patches are seen in the largest area of dark cratered terrain (Figs. 22 and 23). When examined at high resolution (Fig. 25), they are found to be related to ancient impact craters, typically 100 to 300 km in diameter, which have extremely subdued relief. In some of these patches a low annular ridge marks the position of the original crater rim crest; the floor of the crater is essentially at the level of the surrounding terrain. Prominent swarms of smaller secondary craters are preserved around some of the large flattened primary craters. Both the central crater and a surrounding region extending out to the inner margin of the secondary crater zone have an albedo higher than that of the old cratered terrain and about the same as that of the grooved terrain. The relation of the annulus of distinctive albedo to the secondary craters suggests that it corresponds to the continuous deposit of ejecta around large impact craters on the moon and on Mercury. In most but not all of the bright patches, the original crater and its rim have entirely disappeared. All that remains is a circular bright area with a smooth surface that interrupts the older structural grain of the cratered terrain. We propose to call these distinctive smooth bright patches crater palimpsests.

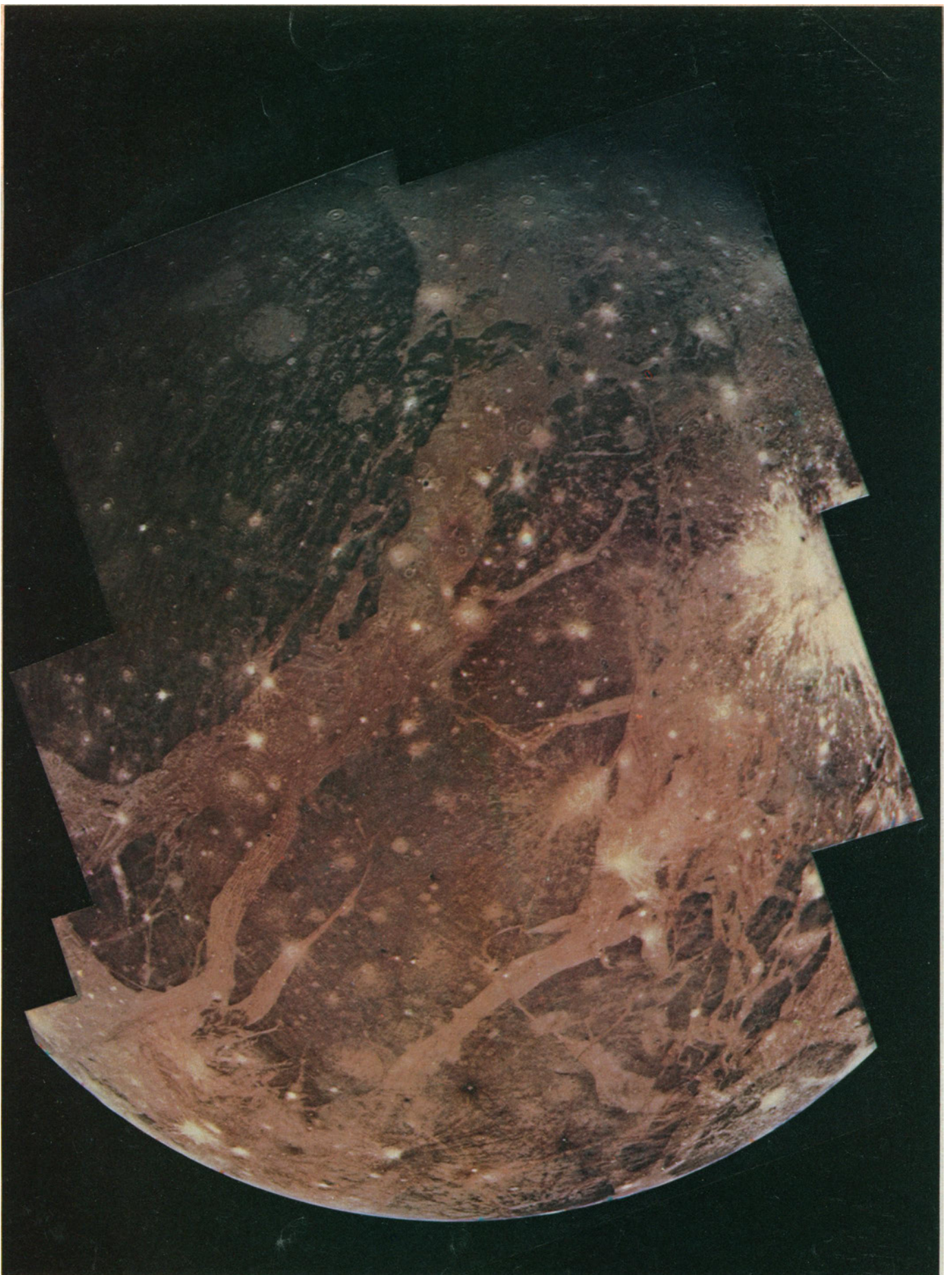


Fig. 23. Color mosaic of Ganymede based on six sets of narrow-angle images in violet, blue, and green acquired from a range of 310,000 km. Well displayed are the ancient, dark, heavily cratered terrain, the networks of younger grooved terrain, and numerous impact craters with bright rays and dark halos. This computer mosaic was prepared by C. C. Avis at the JPL Image Processing Laboratory.

sests: The distribution of crater palimpsests on old cratered terrain suggests that craters larger than 100 km have been produced on Ganymede in about the same proportion to smaller craters as on the moon and on the terrestrial planets, but the number of surviving craters has been substantially reduced by cold flow early in the planet's history (21).

Whereas craters several hundred kilometers in diameter are found only as subdued scars on the oldest parts of Ganymede's surface, craters 50 to 150 km in diameter are relatively abundant on dark cratered terrain and present to a lesser extent on the younger grooved terrain on the hemisphere viewed by Voyager 2 (Fig. 25). Inspection of craters in this size range shows that on the old cratered terrains the craters exhibit a spectrum of morphologies, ranging from featureless palimpsests to sharp-rimmed flat-floored craters, but on the younger grooved terrain most of the craters are much better preserved, having suffered little cold flow of rims and central features. Evidently Ganymede's crust was cooling, becoming thicker and more rigid, from the period of formation of the dark cratered terrain through the evolution of grooved terrain.

Further evidence that Ganymede's crust was rapidly changing and becoming more rigid is provided by a circular impact basin surrounded by an extensive mountainous rim. The feature is centered near -125°W , 60°S (Fig. 26) and resembles some of the major impact basins of the inner solar system, including Orientale and Imbrium on the moon, Caloris on Mercury, and Argyre on Mars. The inner diameter of this relatively flat-floored depression is about 175 km. It is surrounded, out to a distance of about one crater diameter, by closely spaced blocky massifs 20 to 40 km in length, the long axes of which lie radially to the basin. Beyond about one diameter the blocky terrain grades into subdued radial grooves and troughs that extend outward for at least another $1\frac{1}{2}$ diameters. An incomplete and highly irregular, segmented, inward-facing scarp or "ring" structure can be seen on the northwest side of the basin. The radially furrowed terrain in turn grades outward into a smooth ejecta facies that can be recognized as far out as 3 to $3\frac{1}{2}$ diameters from the edge of the inner basin. This material is slightly brighter than the nearby grooved and cratered terrains, which are characteristic of most of the rest of Ganymede. Emerging from beneath the smooth outer ejecta facies are radially oriented chains and clusters of secondary craters much like those seen around

the younger basins of the inner solar system. The secondary craters are clearly superposed on some of the younger grooved terrain, implying that the basin formed after the breakup of the crust and formation of the grooved terrain. The basin is comparable to the basins on the moon and Mars in its topographic freshness and its dense population of large superposed craters. Like the basins of the inner solar system, this feature is probably ancient, several billion years old. Its morphological similarity to basins of the inner solar system suggests that it formed on a relatively rigid crust. Evidently Ganymede's crust had cooled and solidified to a substantial depth early in its history. A major difference between this basin and those in the inner solar system is the radial spacing of the ejecta facies. Here the different facies occur at

much greater distances from the center than do equivalent morphological units around analogous basins of the inner solar system. This occurrence may simply reflect the fact that this basin formed in a crust of ice with a density close to unity, whereas the basins of the inner solar system formed in silicate crusts with densities near 3 g/cm^3 .

Voyager 2 acquired images of the surface of Ganymede at a resolution about three times better than the best achieved by Voyager 1. Shown in the higher resolution data are a variety of complex forms and interrelations within the grooved terrain (Fig. 27). Grooved terrain developed at different rates on opposite sides of what is inferred to be a transform fault (Fig. 27a); some lateral motion may also have occurred along this fault. Grooves and craters were



Fig. 24. Photomosaic of Ganymede taken from a range of 97,000 km (including an area 2000 km in width). A bright-rayed impact crater 150 km in diameter centered near 160°W , 40°S is shown (Fig. 13). The continuous ejecta blanket around the crater is interrupted by two dark areas where the bright material was evidently mixed with dark material at a later time.

formed in overlapping discrete stages in the region illustrated in Fig. 27b; craters were formed earlier than and between several stages of grooved terrain development. Additional evidence for lateral offset of grooved terrain on faults can be seen on the north-south groove set on the left side of Fig. 27b. A distinctive new type of grooved terrain, here called reticulate terrain, has been discovered in

the southern equatorial region near 180°W (Fig. 27c). The reticulate terrain is composed of short ridges and grooves that intersect at angles generally close to 90°. Individual ridges and grooves in this terrain are ~ 5 to 50 km long; the topographic relief is probably only a few hundred meters. The reticulate terrain occurs within polygons as much as a few hundred kilometers across that are en-

closed by normal grooved terrain. In addition to an unusually coarse form of grooved terrain, shown in Fig. 27d, new terrain hinted at by the Voyager 1 data is clearly shown in the higher-resolution Voyager 2 image and is here termed smooth terrain. Smooth terrain replaces or floods sections of the grooved terrain.

Many features on Ganymede suggest that they were formed, at least in part, by normal faulting and local expansion or spreading of the crust. Proof of crustal spreading has been particularly difficult to establish, however. One concrete line of evidence is provided by a crater that is cut by a rimmed trough or fault system in dark cratered terrain and that appears pulled apart (upper left corner of Fig. 27b). Another, less conclusive argument for spreading is the occurrence of apparent transform faults which transect the grooved terrain and across which the width of the grooved terrain changes abruptly. A particularly spectacular example of a transform fault system is illustrated in Fig. 27a.

Callisto. Jupiter's fourth large Galilean satellite was shown by Voyager 1 to have an intensely cratered surface. Craters several tens of kilometers in diameter stand shoulder to shoulder, implying a surface dating back to a period of heavy bombardment (1). Voyager 1 images showed a particularly striking type of feature, consisting of giant concentric rings of subdued bright ridges around a bright featureless central zone. The pattern suggests that large basin-scale impacts disrupted Callisto's crust early in its history. The lack of relief along the bright limb, the absence of a basin and raised rim at the center of the ring systems, and the flat floors and low relief of most large craters (> 50 km in diameter) are consistent with the argument that Callisto, like Ganymede, had a soft icy crust early in its history.

Voyager 2 viewed, at near encounter, the hemisphere opposite that seen by Voyager 1 (Fig. 28). From these two data sets the entire equatorial region has been portrayed on the airbrush base map (Fig. 13c). As can be seen from the high-resolution enhanced mosaic acquired by Voyager 2 (Fig. 28), Callisto is even more densely cratered on this hemisphere than on the sub-Jupiter hemisphere. The only major feature that stands out in the Voyager 2 view is a ringed basin seen by Voyager 1 against the terminator (located at 55°N, 170°W).

Discussion: Relative ages and absolute time scales. One of the primary tools used in establishing geologic histories for the surfaces of the moon and the planets has been measurement of densities of im-



Fig. 25. Photomosaic of Voyager 2 Ganymede images centered near 125°W, 7°N (Fig. 13) and taken at a range of 87,000 km (including an area 1000 km in width). Rimmed furrows that form part of a great ring system on Ganymede somewhat resembling the ring systems of Callisto are well displayed. A variety of impact crater forms are visible, including craters with strong topographic expression, craters that are much degraded, and brighter crater palimpsests (see text) that record the former presence of craters and their surrounding ejecta blankets. The former large craters whose positions are revealed by the palimpsests apparently have disappeared as a result of cold viscous flow in Ganymede's icy crust.

compact craters on the diverse geologic units or terrains of which these surfaces are composed. The greater the number of superposed craters per unit area, the greater the age of a particular surface unit. Such crater density information can be reliably used to establish relative ages among units on one planet, as the cratering rate at a particular time can usually be assumed to be nearly uniform over that planet. Attempting to compare crater densities for surfaces of different planets, in order to establish relative and absolute ages, is far more hazardous; it requires knowledge of the cratering rate history for each of the planets. Although we are faced with the same difficulty in deriving absolute time scales for the Galilean satellites by, say, comparing their crater populations with that of the moon, the Galilean satellites present a third special case. Because they are spatially close together (on a solar system scale), we can fairly reliably establish relative ages of various surface units among the four bodies by taking into account the effects of Jupiter's gravity.

Assembled in Fig. 29 are impact crater size-frequency distributions for various surfaces on the Galilean satellites and representative surfaces on bodies in the inner solar system. The curves have been simplified for clarity. The most densely cratered surface in the Galilean satellite system is that of Callisto, excluding the central regions of the giant ring structures, where the crater densities are down by factors of 2 to 3. This surface is nearly as heavily cratered as the densely cratered highlands of the moon, Mars, and Mercury. The rapid falloff of the crater frequencies at larger diameters on Callisto may reflect collapse of large old craters in an early soft icy crust, or possibly a paucity of impacting objects in this size range.

Ganymede shows a broad spectrum of crater densities ranging from that of the dark cratered terrains, which is comparable to that of Callisto, down to that of the smooth terrain, which is like the crater densities of the lunar maria and old martian plains. The difference in form between the size-frequency distributions of craters found on the dark cratered terrain of Ganymede and the distribution found on Callisto may reflect differences in the rigidity of the early crusts of these two bodies with depth and through time. The grooved terrains on Ganymede show an enormous spread in relative crater density. The oldest grooved terrain has a crater density like that of the dark cratered terrain, indicating that the formation of the grooved terrain began early, while the

ancient dark terrain was being heavily cratered. The youngest of the grooved terrains and the smooth terrain on Ganymede, although a factor of 10 less cratered than the oldest grooved terrain, are about as cratered as average lunar maria and old martian plains.

Only three craters (~ 20 km in diameter) on Europa can be identified as prob-

able impact craters. As noted earlier, numerous smaller circular depressions (5 to 15 km in diameter) are visible but their genesis is unclear. Hence we have a single point on the size-frequency plot for Europa in Fig. 29; the slope of the crater size-frequency distribution is unknown. Interestingly, there is about the same density of terrestrial impact craters

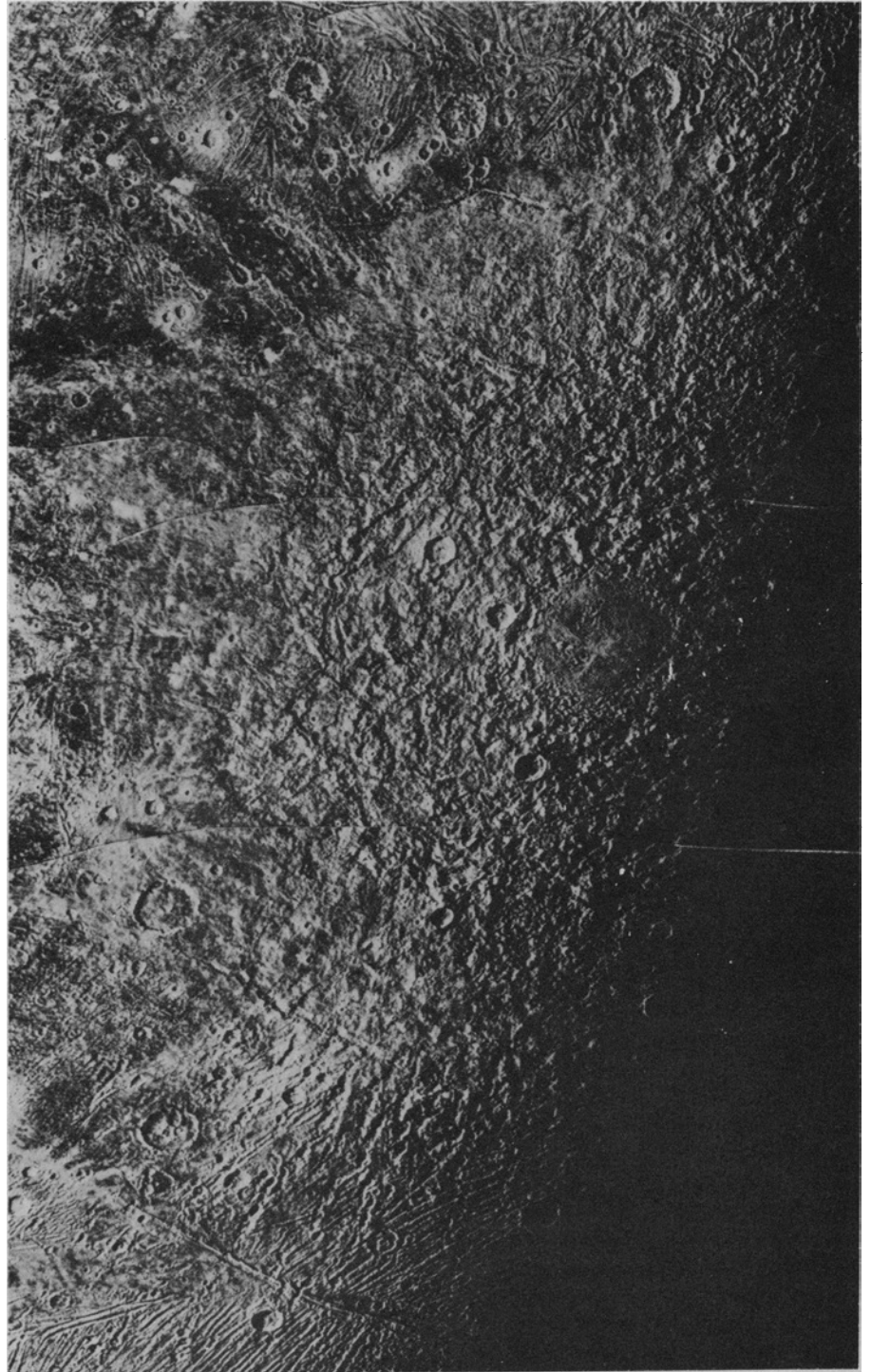


Fig. 26. Photomosaic of Ganymede taken from a range of 70,000 km (including an area 1000 km in width). A fresh impact basin 175 km in diameter centered near 125°W, 60°S (see Fig. 13) is shown surrounded by an ejecta deposit that grades outward from radial furrowed terrain to smooth ejecta in a distance of three crater diameters. This basin has large topographic relief and differs drastically from the recognizable large craters on Ganymede. Evidently it formed when the crust of Ganymede had become rigid and capable of sustaining major relief.

of Phanerozoic age (< 600 million years) in this size range on the stable continental shields (26). The slope of the curve for Earth probably reflects the difficulty in finding smaller craters as well as the dynamic effects of erosion and sediment transport on Earth.

The upper limit of crater density for Io (Fig. 24) is taken from Johnson *et al.* (27); this limit is derived from resolution thresholds for crater detection and the areal coverage of high-resolution images. As noted by Smith *et al.* (1), no impact craters were detected on Io. The curve in Fig. 29 reinforces the observation that Io's surface is the least cratered and possibly the youngest and most geologically

Table 2. Relative cratering rates on the Galilean satellites for $V_{\infty} = 8$ km/sec.

Satellite	Flux concentration by Jupiter gravity	Mean impact velocity (km/sec)	Crater production rate relative to Callisto
Callisto	3.3	14	1
Ganymede	5.0	18	2.0
Europa	7.3	21	2.8
Io	11.1	26	5.3

active surface in the solar system. Even the western deserts of the United States have a greater crater density; Meteor Crater (1.5 km in diameter) in Arizona is only about 30,000 years old.

The first-order question to be solved in establishing an absolute chronology from the crater density data in Fig. 29 concerns the impact histories of the Galilean satellites relative to the impact histories in the inner solar system; in particular, rates of impact relative to those on the moon and Earth need to be established. The number of Mars-crossing asteroids deflected into Jupiter's vicinity is about the same as the number deflected into the vicinity of Earth (1); however, the residence time of these bodies near Jupiter is probably very short and they have a relatively minor effect. In that case, the flux of impacting bodies near Jupiter is probably dominated by comet nuclei. We now estimate the flux of impacting objects at Jupiter's heliocentric distance to be at least a factor of 10 (and possibly a factor of 100) lower than that for the moon. Jupiter itself, however, dramatically alters the crater production rate implied by this flux. Both deflected Mars-crossing asteroids and periodic comets will have incoming velocities relative to Jupiter and the satellites of 10 km/sec. Using the mean encounter velocity outside Jupiter's sphere of influence for periodic comets (V_{∞}) of 8 km/sec, we summarize the relative crater production rates on the satellites in Table 2.

We arrive at the following general conclusions:

1) The cratered terrains on Ganymede and Callisto certainly must date back to the late torrential bombardment period some 4 billion years ago, as do the cratered highlands of the moon, regardless of whether the recent fluxes have been roughly the same for Ganymede and Callisto as for the moon (1) (which we now suspect to be an overestimate) or substantially less.

2) Formation of grooved terrain started during this torrential bombardment period and, given the same range of impact fluxes relative to the moon, probably lasted less than a few hundred million years.

3) Europa's surface must be at least 10^8 years old if the flux of impacting bodies near Jupiter is similar to that near Earth and the moon, even allowing for the enhancement of the flux by Jupiter's gravity. If the flux on Europa is far less than that on the moon, as we now suspect, Europa's surface may be several billion years old. Europa may have

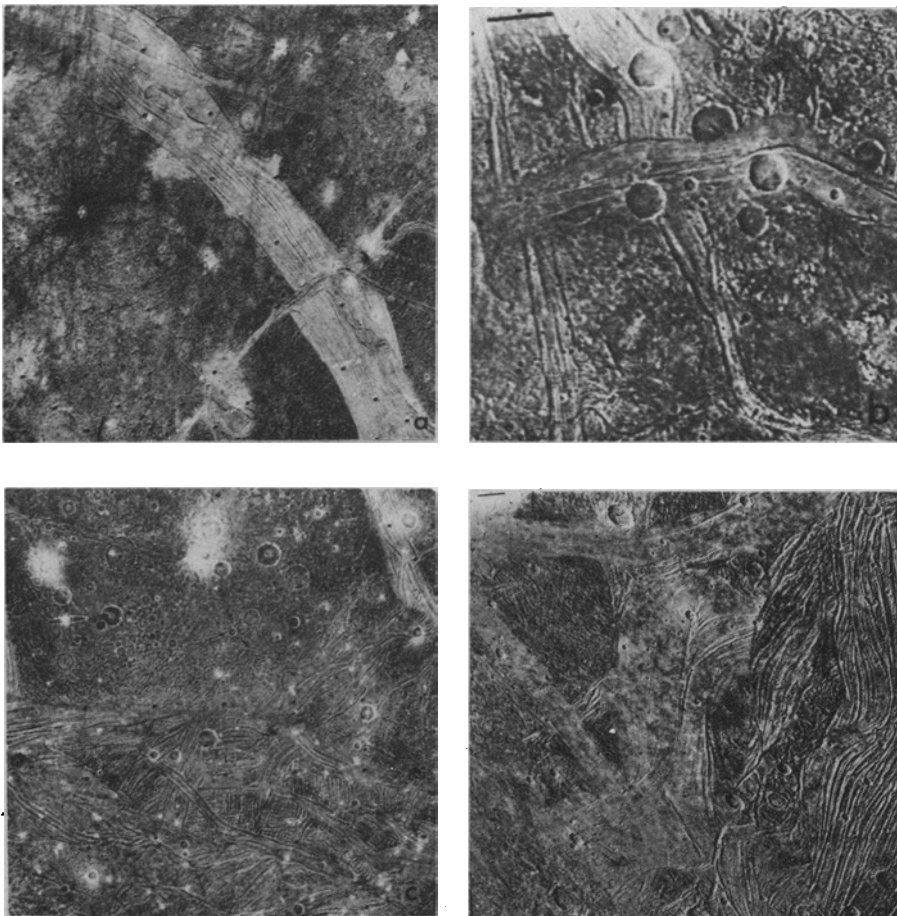


Fig. 27. Variants of grooved and smooth terrain on Ganymede. (a) Image of Ganymede centered near the equator at 210° W (including an area 900 km in width) showing a bright strip of grooved terrain apparently cut by a fault. The width and number of grooves differ on the two sides of the fault (14 on the north; 20 on the south). One explanation is that the grooves formed on successive fractures in the crust at different rates on opposite sides of the fault. Also shown are craters with dark halos, where dark material has evidently been excavated from the crust. (b) Image centered near 135° W, 25° S (including an area 300 km in width) showing many transecting strands of grooved terrain with impact craters that were formed after, before, and during the development of the grooved terrain. (c) An unusual reticulate network of grooved terrain centered near 165° W, 15° S (including an area 600 km in width) can be seen in the lower part of this frame. Here elements of grooved terrain butt against one another orthogonally. Also visible in the upper left corner is a striking case in which a crater in the dark cratered terrain has been spread apart by a furrowed trench that intersects it. (d) Moderately cratered grooved terrain cutting the older, darker, heavily cratered terrain is shown here centered near 205° W, 72° S (including an area 500 km in width). In the middle is a terrain that is markedly smoother than other areas. This smooth terrain may be due to flooding of the surface with material that covered the grooves.

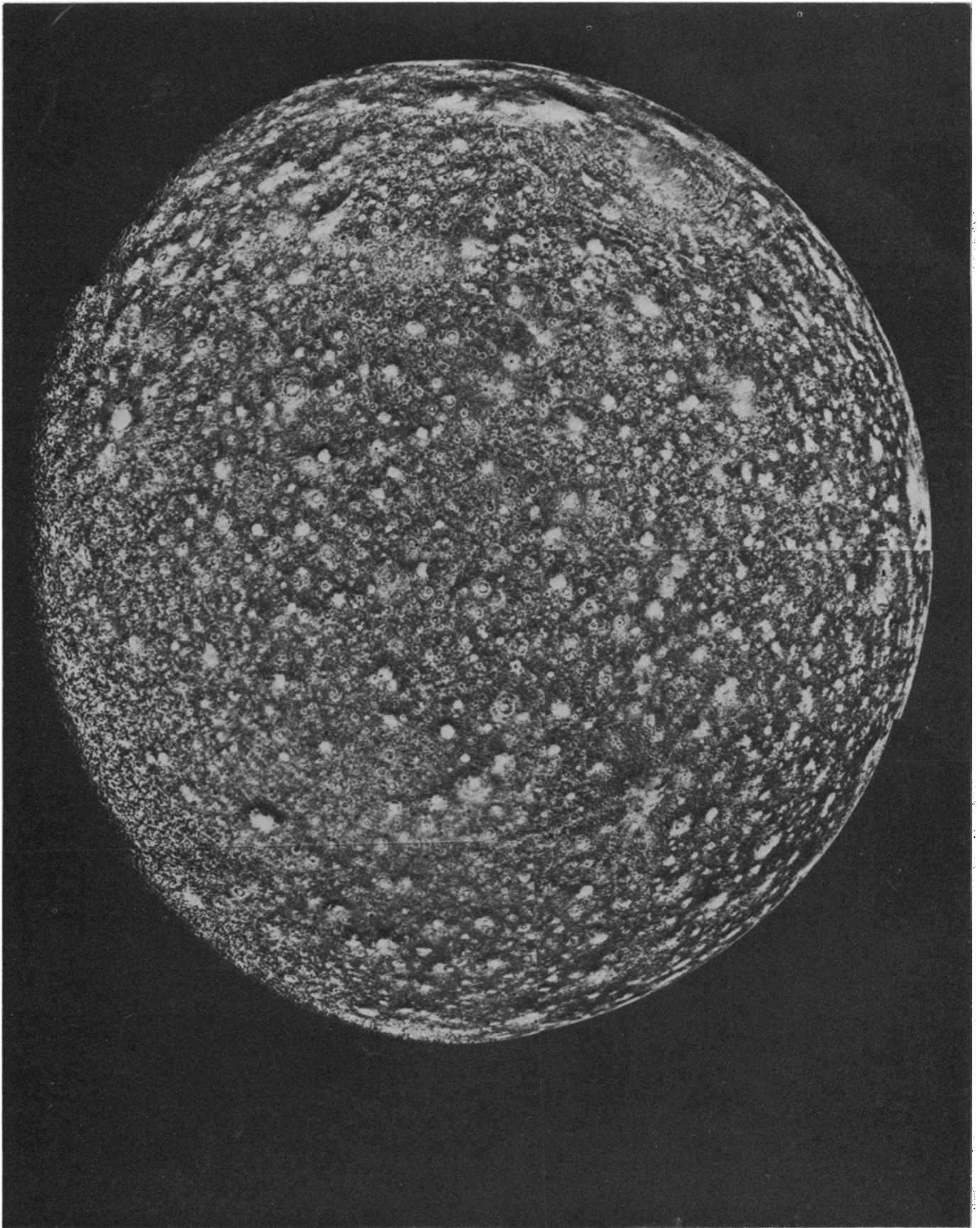


Fig. 28. Photomosaic of Callisto taken from a range of 390,000 km. The impact crater distribution is relatively uniform across the disk. Notable are the bright-rayed craters. Near the upper right limb a large ring structure can be seen (centered near 140°W, 30°N; Fig. 13). Part of this structure was seen by Voyager 1. About 15 concentric rings surround the central bright patch.

frozen once, after the torrential bombardment was over, and simply been subjected to continual erosion by sputtering since that time. In fact, the crater density on Europa gives us a lower limit for the flux after the torrential bombardment. Europa's surface cannot be more than 4.5 billion years old or it would show scars of large ancient craters formed during that bombardment. This gives a lower limit (three craters in 4.5 billion years) of about one-tenth the lunar cratering rate.

4) Enhancement by Jupiter's gravity makes the Io crater production rate close to or greater than the present cratering rate on the moon, using a plausible range of crater production rates at Jupiter's heliocentric distance. Hence, the ab-

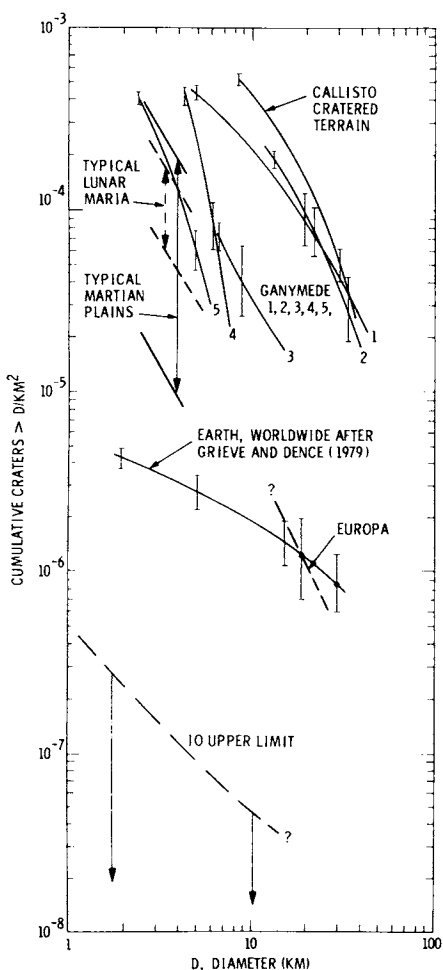


Fig. 29. Cumulative size-frequency distributions of craters on the Galilean satellites compared with the size-frequency distributions of craters on the surfaces of the moon and terrestrial planets. The number of craters larger than a given diameter (D) per unit area is plotted. The Callisto curve represents the densely cratered regions that dominate its surface. Shown for Ganymede are: 1, old cratered terrain; 2, old grooved terrain; 3 and 4, intermediate grooved terrain; and 5, smooth terrain. The crater distribution on the continental shield areas of Earth is from Grieve and Dence (26).

sence of craters on Io strongly indicates that it must be the youngest and most dynamic surface in the solar system.

BRADFORD A. SMITH
Department of Planetary Sciences,
University of Arizona, Tucson 85721

LAURENCE A. SODERBLOM
U.S. Geological Survey,
Flagstaff, Arizona 86001

RETA BEEBE
Department of Astronomy,
New Mexico State University,
Las Cruces 88003

JOSEPH BOYCE
GEOFFREY BRIGGS
NASA Headquarters,
Washington, D.C. 20546

MICHAEL CARR
U.S. Geological Survey,
Menlo Park, California 94025

STEWART A. COLLINS
Jet Propulsion Laboratory,
Pasadena, California 91103

ALLAN F. COOK II
Smithsonian Astrophysical Observatory,
Cambridge, Massachusetts 02138

G. EDWARD DANIELSON
Division of Geological and Planetary
Sciences, California Institute of
Technology, Pasadena 91125

MERTON E. DAVIES
Rand Corporation,
Santa Monica, California 90406

GARRY E. HUNT
University College London,
London WC 1E 6BT, England

ANDREW INGERSOLL
Division of Geological
and Planetary Sciences,
California Institute of Technology

TORRENCE V. JOHNSON
Jet Propulsion Laboratory

HAROLD MASURSKY
JOHN MCCAULEY
U.S. Geological Survey, Flagstaff

DAVID MORRISON
Institute for Astronomy, University
of Hawaii, Honolulu 96822

TOBIAS OWEN
Department of Earth and Space
Sciences, State University of New York,
Stony Brook 11790

CARL SAGAN
Cornell University,
Ithaca, New York 14853

EUGENE M. SHOEMAKER
U.S. Geological Survey, Flagstaff

ROBERT STROM
Lunar and Planetary Laboratory,
University of Arizona

VERNER E. SUOMI
Space Science and Engineering Center,
University of Wisconsin,
Madison 53706

JOSEPH VEVERKA
Cornell University

References and Notes

- B. A. Smith, L. A. Soderblom, T. V. Johnson, A. P. Ingersoll, S. A. Collins, E. M. Shoemaker, G. E. Hunt, H. Masursky, M. H. Carr, M. E. Davies, A. F. Cook II, J. Boyce, G. E. Danielson, T. Owen, C. Sagan, R. F. Feebe, J. Veverka, R. G. Strom, J. F. McCauley, D. Morrison, G. A. Briggs, V. E. Suomi, *Science* **204**, 951 (1979).
- T. Gehrels, in *Jupiter*, T. Gehrels, Ed. (Univ. of Arizona Press, Tucson, 1976), p. 206.
- B. A. Smith and G. E. Hunt, in *Jupiter*, T. Gehrels, Ed. (Univ. of Arizona Press, Tucson, 1976), p. 564; R. J. Terrile and R. F. Beebe, *Science* **204**, 948 (1979).
- B. M. Peek [*The Planet Jupiter* (Faber & Faber, London, 1958)] presents a detailed explanation of this nomenclature.
- A. P. Ingersoll et al., *Nature (London)* **280**, 773 (1979).
- J. L. Mitchell et al., *ibid.*, p. 776.
- See figure 5 in (1).
- G. E. Hunt and J.-P. Muller, *Nature (London)* **280**, 778 (1979).
- A. F. Cook II, T. C. Duxbury, G. E. Hunt, *ibid.*, p. 780.
- ibid.*, p. 794.
- T. Owen, G. E. Danielson, A. F. Cook II, C. Hansen, V. L. Hall, T. C. Duxbury, *ibid.* **281**, 442 (1979).
- R. Beer and F. W. Taylor, *Astrophys. J.* **221**, 1100 (1978).
- D. C. Jewitt, G. E. Danielson, S. P. Synnott, *Science* **206**, 951 (1979).
- L. A. Morabito, S. P. Synnott, P. N. Kupferman, S. A. Collins, *ibid.* **204**, 972 (1979).
- R. Hanel et al., *ibid.*, p. 972.
- C. B. Pilcher, S. T. Ridgway, T. B. McCord, *ibid.* **170**, 1087 (1972).
- F. P. Fanale, T. V. Johnson, D. L. Matson, in *Planetary Satellites*, J. A. Burns, Ed. (Univ. of Arizona Press, Tucson, 1977), p. 379.
- G. J. Consolmagno and J. S. Lewis, in *ibid.*, p. 492.
- P. M. Cassen, R. T. Reynolds, S. J. Peale, *Geophys. Res. Lett.* **6**, 731 (1979).
- R. T. Reynolds and P. M. Cassen, *ibid.* **6**, 121 (1979).
- T. V. Johnson and T. R. McGetchin, *Icarus* **18**, 612 (1973).
- D. L. Matson, T. V. Johnson, F. P. Fanale, *Astrophys. J.* **192**, L43 (1974).
- W. L. Brown et al., *Phys. Rev. Lett.* **40**, 1027 (1978).
- L. J. Lanzerotti et al., *Geophys. Res. Lett.* **5**, 155 (1978).
- N. Purves and C. B. Pilcher, in press.
- R. A. F. Grieve and M. R. Dence, *Icarus* **38**, 230 (1979).
- T. V. Johnson, A. F. Cook II, C. Sagan, L. A. Soderblom, *Nature (London)* **280**, 746 (1979).
- Several of the observations reported here were possible only because the Voyager Project Office permitted major, last-minute redesign of Voyager 2's near-encounter command load to increase observations of various features discovered by Voyager 1. Many individuals contributed significantly to this successful effort, with J. S. Carter, C. J. Hansen, W. A. Magoon, and S. J. Zawacki playing key roles. The success of this experiment is a tribute to the extraordinary efforts of the hundreds of individuals, throughout the world, who have devoted their considerable talents to this undertaking. Among those who contributed most directly to the Voyager 2 Jupiter imaging operations are: J. L. Mitchell (Jupiter observational design and subsequent velocity measurement); P. N. Kupferman (exposure determination); J. L. Anderson, A. L. Lane, C. H. Stemberge, and the personnel of the Voyager Sequence Team and the Mission Imaging Operations Group (data acquisition and processing); C. C. Avis, G. W. Garneau, P. L. Jepsen, E. P. Korsmo, J. A. Mosher, A. A. Schwartz, and G. M. Yagi (image processing); R. Batson, P. Bridges, P. Collins, J. Inge, C. Isbell, B. K. Luchitta, D. C. Pieri, G. G. Schaber, and R. Tyner (analysis and cartography); R. Gurr, J. T. Harwood, V. J. Nelson, L. J. Pieri, F. Popescu, D. Simonelli, and the Jet Propulsion Laboratory (JPL) Photolab (operational support); and M. J. S. Belton, M. Flasar, H. Kieffer, M. C. Malin, and R. J. Terrile for their careful reviews of this manuscript. G. E. Hunt is supported by the Science Research Council, Great Britain. This is contribution 3325 of the Division of Geological and Planetary Sciences, California Institute of Technology. This report presents the results of one phase of research carried out at JPL under NASA contract NAS 7-100.